

**HUGHES**

AIRCRAFT COMPANY

ELECTRON DYNAMICS DIVISION

CR#171977

**NASA CONTRACTOR REPORT  
INTERIM TECHNICAL REPORT**

**ADVANCED RADIATOR CONCEPTS  
UTILIZING HONEYCOMB PANEL  
HEAT PIPES (STAINLESS STEEL)**

(NASA-CR-171977) ADVANCED RADIATOR CONCEPTS  
UTILIZING HONEYCOMB PANEL HEAT PIPES  
(STAINLESS STEEL) Interim Technical Report  
(Hughes Aircraft Co.) 78 p

CSCI 20D

N87-16785

Unclas

G3/34 43731

CONTRACT NAS 9-16581  
W-30746

**NASA CONTRACTOR REPORT  
INTERIM TECHNICAL REPORT**

**ADVANCED RADIATOR CONCEPTS  
UTILIZING HONEYCOMB PANEL  
HEAT PIPES (STAINLESS STEEL)**

CONTRACT NAS 9-16581  
W-30746

**PREPARED FOR**

**NATIONAL AERONAUTICS AND SPACE ADMINISTRATION  
LYNDON B. JOHNSON SPACE CENTER  
HOUSTON, TEXAS 77058**

**G. L. FLEISCHMAN  
H. J. TANZER**

**AUGUST 1985**

**HUGHES AIRCRAFT COMPANY  
ELECTRON DYNAMICS DIVISION  
3100 WEST LOMITA BOULEVARD  
P.O. BOX 2999  
TORRANCE, CA 90509-2999**

# NOMENCLATURE

$A_w$	Wick cross-sectional flow area
$D$	Honeycomb core depth
$g$	Acceleration due to gravity
$K$	Permeability of wick
$L$	Length
$L_{eff}$	Effective length of heat pipe
$Q_{max}$	Quantity of heat, maximum
$Q_e$	Entrainment limit
$Q_s$	Sonic limit
$Q_w$	Wicking limit
$TF_\ell$	Liquid tortuosity factor
$TF_v$	Vapor tortuosity factor
$MF\Delta P$	Localized pressure drop magnification
$\Delta P_T$	Total pressure drop
$\Delta P_n$	Pressure drop of $n = 1, 2, 3, \dots$
$\Delta P_c$	Capillary head pressure difference
$\Delta P_g$	Pressure drop due to gravity
$\Delta P_\ell$	Pressure drop in the liquid
$\Delta P_v$	Pressure drop in the vapor
$r_c$	Effective capillary radius
$r_v$	Hydraulic radius of vapor space
$\theta$	Contact angle
$\lambda$	Latent heat of vaporization
$\mu_\ell$	Dynamic viscosity of liquid
$\mu_v$	Dynamic viscosity of vapor
$\rho_\ell$	Density of liquid
$\rho_v$	Density of vapor
$\sigma$	Surface tension

PRECEDING PAGE BLANK NOT FILMED

## FOREWORD

This interim report was prepared by the Hughes Aircraft Company, Electron Dynamics Division, for the NASA Johnson Space Center.

The purpose of this program was to determine the feasibility of using honeycomb panel heat pipes as reliable, lightweight and highly efficient radiators for future space station applications. The scope of this program includes the design, fabrication, testing and delivery of two prototype heat pipe panels, which are 24 inches (0.61 m) wide by 120 inches (3.0 m) long. This interim report describes the first unit, which was fabricated from stainless steel. The second panel shall be fabricated from aluminum. Upon completion of the aluminum unit testing a final technical report will be prepared.

This program is being conducted in accordance with the Statement of Work in NASA Contract NAS9-16581. Mr. G. L. Fleischman is the Hughes, Electron Dynamics Division, Project Manager while Mr. A. Basiulis serves as both administrative and technical adviser at Hughes. Mr. H. J. Tanzer was responsible for the stainless steel honeycomb panel heat pipe design, analysis and fabrication. Mr. J. T. Burdette was responsible for heat pipe processing and testing. Technical direction was provided by Mr. J. G. Rankin, Technical Representative, NASA Johnson Space Center.

**PRECEDING PAGE BLANK NOT FILMED**



## TABLE OF CONTENTS

<u>Section</u>	<u>Page</u>
1.0 SUMMARY	1
2.0 INTRODUCTION	3
3.0 DESIGN EVALUATION	5
3.2 The Honeycomb Panel Heat Pipe Fin	5
3.2.1 Concept	5
3.2.2 Manufacturing Technology Status	8
3.2.3 Design Details and Constraints	11
3.3 Analysis	15
3.4 Final Design	18
4.0 FABRICATION	25
4.1 Pieceparts	25
4.1.1 Diffusion Welded Material	25
4.1.2 Core Ribbon Fabrication	25
4.1.3 Panel Facesheet Joining	27
4.2 Honeycomb Panel	29
5.0 TEST PERFORMANCE	33
5.1 Test Setup	33
5.2 Processing Procedures	37
5.3 Test Results	38
5.3.1 Ambient Air Testing	38
5.3.2 Performance Testing Over the Temperature Range -4 to 149°F (-20 to 65°C)	42
5.3.3 Liquid Fill Test	46
5.3.4 Tilt Test	48
5.3.5 Burst Pressure Test	52
6.0 DATA CORRELATION AND CONCLUSIONS	57
6.1 Data Correlation	57
6.2 Conclusions	65

PRECEDING PAGE BLANK NOT FILMED

# LIST OF ILLUSTRATIONS

<u>Figure</u>		<u>Page</u>
1	Sketch of space radiator element.	6
2	Original requirements and test conditions.	6
3	Honeycomb heat-pipe panel concept.	7
4	Core ribbon details	12
5	Sketch of heat-pipe honeycomb panel.	14
6	Panel manufacture constraints.	14
7	Liquid flow path schematic diagram: 1 cell.	17
8	Flange section liquid flow model.	19
9	Performance limits vs temperature for 1 inch thick honeycomb cell panel.	20
10	Performance limits vs temperature for 0.25 inch thick honeycomb cell panel.	21
11	Performance limits vs temperature for 0.25 inch thick honeycomb channel panel.	22
12	Panel performance vs panel thickness.	23
13	Comparison between initial and final panel designs.	24
14	Cross section of facesheet/sintered wick interface (250X).	26
15	Core ribbon material after crimping.	26
16	Butt welded face sheet sample showing sintered screen wick.	28
17	Butt welded (GTAW) face sheets for heat pipe.	28
18	Close-up of internal honeycomb structure.	30
19	Completed honeycomb panel.	31
20	Performance test set-up.	34
21	Schematic diagram of test station.	35
22	Honeycomb panel performance test instrumentation.	36
23	Performance test temperature distribution at 180 watts heat input.	39

# LIST OF ILLUSTRATIONS (CONTINUED)

<u>Figure</u>		<u>Page</u>
24	Strip chart temperature recording at 400 watts.	40
25	Temperature recording at 400 watts after removal of trapped liquid in corner (6, 24).	41
26	Temperature recording at 100 watts (Cost Test).	44
27	Temperature recording at 500 watts (Elevated Temperature).	45
28	Temperature recording at 400 watts (110% fill).	47
29	Maximum heat transport capacity test (130% fill).	49
30	Verification of excess liquid in corner identified as 6, 24 (130% fill).	50
31	Verification of excess liquid in corner identified as 17, 29 (130% fill).	51
32	Honeycomb panel heat pipe tilt test performance.	53
33	Burst pressure test.	54
34	Honeycomb panel shown as comprised to "unit cells".	59
35	Predicted performance limits upgrade for stainless steel/methanol honeycomb heat pipe.	62
36	Data correlation: thermal transport limitation.	63
37	Data correlation: tilt test performance.	64
38	Summary of cell hole pattern effect on vapor flow direction.	67
39	Detail view of panel section having mixed direction channels.	68
40	Predictions for as-designed and increased capacity designed using correlated model.	71

## LIST OF TABLES

<u>Table</u>	<u>Page</u>
1      Manufacturing Limit	10
2      Preliminary Design Summary; Basis for Analytical Modeling	10
3      Honeycomb Cell Trade-Off Parameters	16
4      Details of Wicking Limitations: Differential Pressure Balance Relationship	16
5      Honeycomb Panel Temperature Distribution at 100 WATTS (Cold Test)	43
6      Honeycomb Panel Temperature Distribution at 500 Watts (Elevated Temperature)	43
7      Summary of Burst Pressure Data	55
8      Summary of Analysis Upgrading	58
9      Summary of Predicted Pressure Losses	65

## 1.0 SUMMARY

The feasibility of fabricating and processing moderate temperature range heat pipes in a low mass honeycomb sandwich panel configuration for highly efficient radiator fins for the NASA space station was investigated. A variety of honeycomb panel facesheet and core-ribbon wick concepts were evaluated within constraints dictated by existing manufacturing technology and equipment. Concepts evaluated include: type of material, material and panel thicknesses, wick type and manufacturability, liquid and vapor communication among honeycomb cells, and liquid flow return from condenser to evaporator facesheet areas. In addition, the overall performance of the honeycomb panel heat pipe was evaluated analytically.

A thin-wall (0.018 inch), all-welded stainless steel design was used for the initial prototype unit described in this report. Stainless steel has excellent weldability and forming properties. Methanol was selected as the working fluid because of its favorable thermal characteristics and vapor pressure over the  $-4$  to  $149^{\circ}\text{F}$  ( $-20$  to  $65^{\circ}\text{C}$ ) temperature range, and compatibility with the stainless steel envelope material. The design goal was to build a 12 inch wide by 240 inch long (0.30 m x 6.10 m) panel that could dissipate 1000 watts over the  $-4$  to  $149^{\circ}\text{F}$  temperature range at 1g test conditions.

In the interest of minimizing weight, the thinnest core depth of 0.25 inch (6.35 mm) and the largest hexagonal cell size within manufacturing limits of 0.50 inch (12.70 mm) were chosen for construction. The hexagonal cell was chosen over channels because of prior experience in the fabrication of this type of heat pipe and the ability to operate the panel in either the longitudinal or transverse direction. A single layer of 120 mesh stainless steel screen was diffusion bonded to the facesheet for good thermal conductance. A porous sintered screen core, perforated to allow vapor communication, was selected for improved transport capacity over the screen/foil core material.

Originally the test panel was intended to be 12 inches wide by 240 inches long (0.30 m x 6.10 m) with a 0.50 inch (12.70 mm) wide heater running the entire length along one edge of the panel. However, these requirements were modified,

as a result of the design evaluation. The honeycomb panel manufacturer\* is currently machine limited to a maximum uninterrupted length of 120 inches (3.05 m). Therefore, the panel length was reduced to 120 inches (3.05 m), and the width was doubled to 24 inches (0.61 m). The heater was relocated to a 1 inch (2.54 cm) wide strip along the centerline of the top surface. This revised test condition maintained the same heat input flux of  $8.33 \text{ W/in.}^2$  ( $1.29 \text{ W/cm}^2$ ), as before, and more realistically simulated an actual space radiator fin application. In this configuration the panel delivered a maximum power of 600 watts at an operating temperature of  $122^\circ\text{F}$  ( $50^\circ\text{C}$ ). The predicted value was 500 watts. The panel was isothermal throughout the entire surface to within  $\pm 3.6^\circ\text{F}$  ( $\pm 2^\circ\text{C}$ ), except for a 6 by 6 inch ( $0.15 \times 0.15 \text{ m}$ ) zone in one corner. As discussed further in this report, this particular corner was thermally isolated from the active panel. It is felt that this was related to the fact that vapor holes were placed only in alternate crimps of the core ribbon material rather than every crimp.

Additional tilt testing was performed by relocating the heater along one edge of the panel. Maximum powers of 70 watts and 50 watts were demonstrated at a panel elevation of 1/2 inch (12.70 mm) and 1.0 inch (2.54 mm), respectively. The corresponding predicted values were 77 watts and 59 watts.

The stainless steel honeycomb panel described in this report weighed  $1.9 \text{ lbs/ft}^2$  ( $9.2 \text{ kg/m}^2$ ). A 5 1/2 inch by 5 1/2 inch ( $0.14 \times 0.14 \text{ m}$ ) subscale honeycomb panel was subjected to a burst pressure test. The core material failed in tension at an internal pressure of 250 psi ( $17.2 \times 10^5 \text{ N/m}^2$ ). The failure was in the wires of the core wick material adjacent to the spotwelds. This shows that honeycomb panels of even higher internal pressure capability can be designed and constructed in the future. Other recommendations for improved designs are given in the Conclusions, Section 6.0, of this report.

---

\* Astech<sup>R</sup>, Division of the TRE Corp., Santa Ana, California

## 2.0 INTRODUCTION

Future space systems will have power and heat rejection requirements that existing technology cannot effectively handle. From a heat rejection viewpoint, a completely new radiator system approach was suggested.<sup>1</sup> The concept consists of a multikilowatt power module comprised of many high-capacity (~2 kw), large (~50 ft. long x 2 ft. wide) heat pipe radiator elements, each independently coupled to a centralized fluid heat source. This modular building-block approach would allow for construction of any desired size radiator system, and for easy on-orbit maintenance and replacement. NASA has initiated development of this approach, which became known as the Space Constructible Radiator (SCR). In an initial study on manned platforms<sup>2</sup> and an extension which focused on unmanned platforms,<sup>3</sup> development of constructible radiator technology was judged to have significant potential for heat rejection system level improvements. This includes high-capacity heat pipes, efficient "plug-in" contact heat exchangers, and lightweight efficient radiator fins.<sup>4</sup>

As the performance of large heat pipes continues to increase, a corresponding improvement must be made in the efficiency of longer radiating fins in order to be able to make use of the heat pipe's maximum transport capabilities and therefore minimize the total number of heat pipes required for a given total system size. The purpose of this program is to investigate the feasibility of using the honeycomb heat pipe<sup>5</sup> as reliable, lightweight and highly efficient space radiator fins.<sup>6</sup> The program objective is to design, fabricate, test and evaluate a representative segment of a full sized radiator fin. The program consisted of the following phases:

- I - Analysis and Preliminary Design
- II - Final Design and Materials Procurement
- III - Fabrication
- IV - Test

This document describes the results of the work performed in each phase.

### 3.0 DESIGN EVALUATION

#### 3.1 REQUIREMENTS

As the modular SCR system is presently perceived, the condenser of the monogroove high capacity heat pipe<sup>7</sup> is imbedded in a double-sided radiator fin, as illustrated in Figure 1. The honeycomb fin picks up heat at the interface with the condenser section of the monogroove heat pipe, and then distributes heat over the surface of the radiating fin.

The program requirements are to design, fabricate, test, and evaluate a representative segment of a full sized radiator fin. Original panel dimensions were nominally set at 240 in. (6.10 m) long by 12 in. (0.30 m) wide. Performance requirements were to dissipate 1000 W over the temperature range of -4 to 149°F (-20 to 65°C) at 1 g test conditions. Heat input was to be along one of the long panel edges, and to be transported in the short in-plane direction. The original requirements and test conditions are shown in Figure 2. These requirements were modified as a result of the design evaluation, and the final test configuration is presented in Figure 13b.

#### 3.2 THE HONEYCOMB PANEL HEAT PIPE FIN

##### 3.2.1 Concept

The heat pipe panel, shown schematically in Figure 3, consists of a wickable honeycomb core, internally wickable facesheets, and an appropriate working fluid. Evaporation of the working fluid occurs at any section of the panel exposed to heating. Vapor will flow to a cooler region where it condenses, and the condensate will return to the evaporator by means of capillary pumping action of the wick structure. The honeycomb cells can be notched at both ends, to allow intercellular liquid flow along the faces, and perforated to allow intercellular vapor flow. The intercellular communication of liquid and vapor is necessary to ensure heat pipe action both in the plane of the panel and through its depth. The primary mode of heat transfer can be either transverse (face-to-face) or longitudinal (in-plane), with the degree in either mode

~~PRECEDING PAGE BLANK NOT FILMED~~



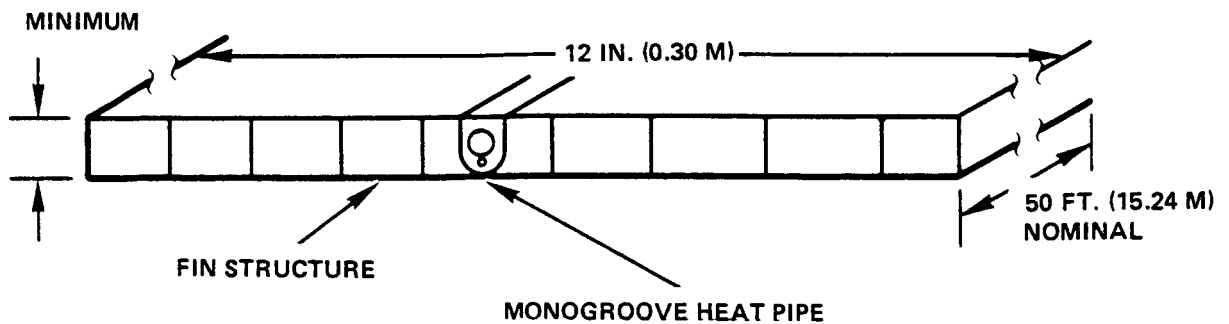


Figure 1 Sketch of space radiator element.

$$Q_{IN} = 1000 \text{ W HEAT INPUT AREA} = 2 (0.5 \times 120 \text{ IN.}) = 120 \text{ IN}^2 (774.19 \text{ CM}^2)$$

$$\frac{Q}{A} = \frac{1000 \text{ W}}{120 \text{ IN}^2} = 8.33 \text{ W/IN}^2 (1.29 \text{ W/CM}^2)$$

#### PANEL DIMENSIONS

LENGTH (L): 240 IN. (6.10 M)

WIDTH (W): 12 IN. (0.30 M)

DEPTH (D): TBD

#### TEST ORIENTATION

EVAP 0.125 IN. (3.18 MM) ABOVE COND

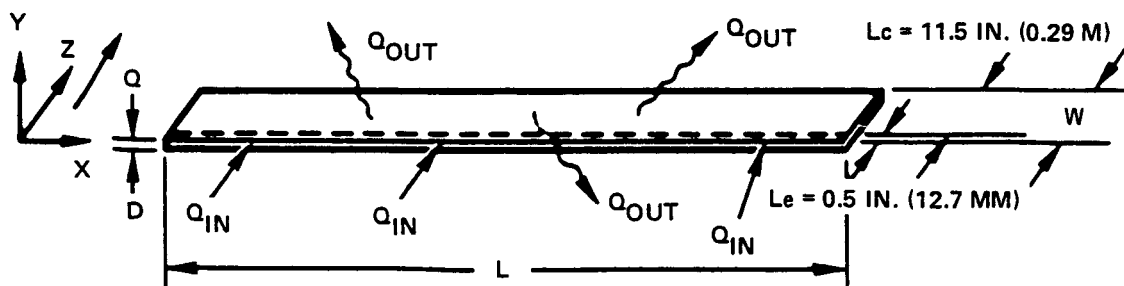


Figure 2 Original requirements and test conditions.

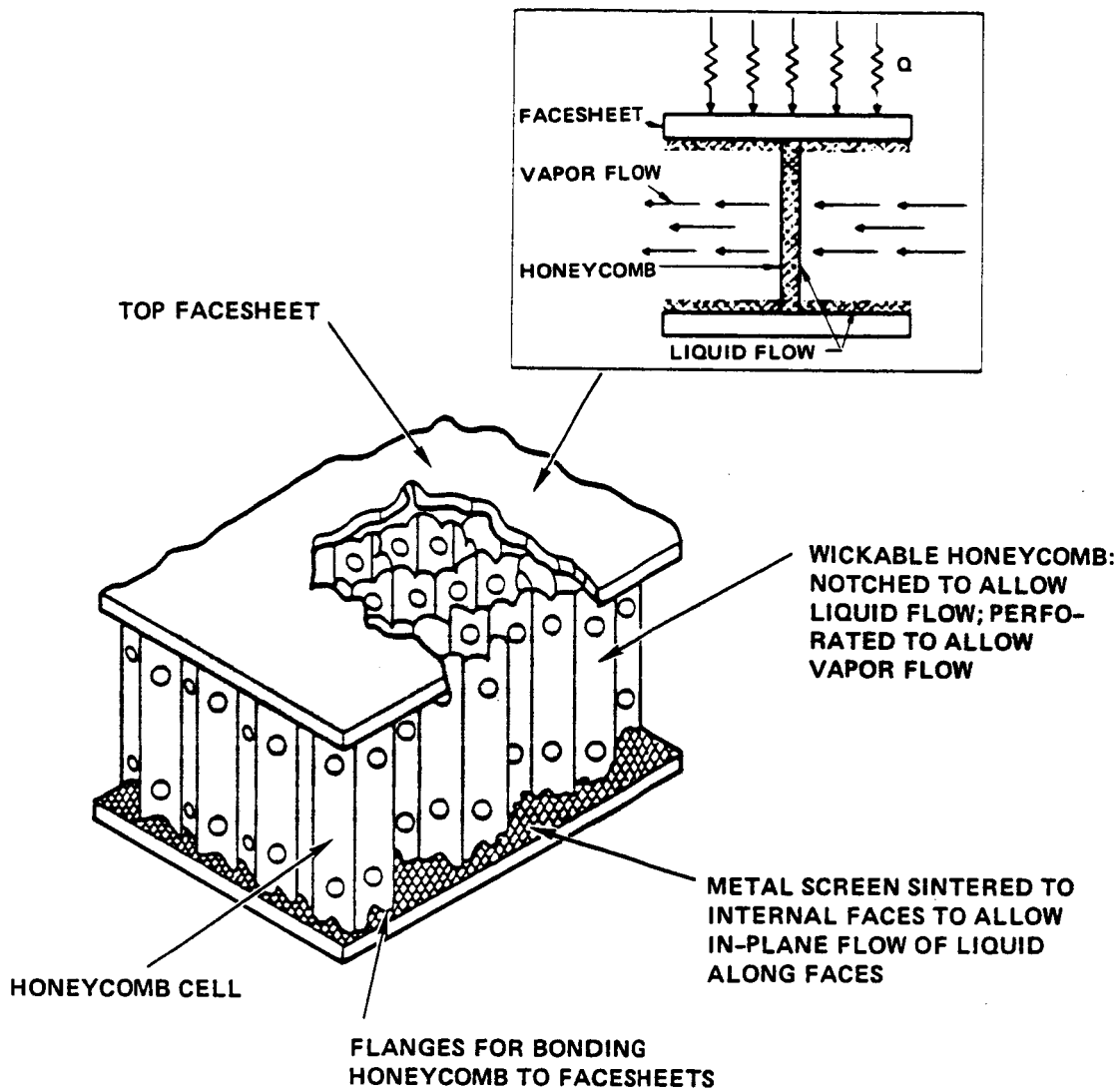


Figure 3 Honeycomb heat-pipe panel concept.

varying with the wickable core design. The present radiator application will require a wickable core design to enhance the longitudinal heat transfer capability. Applying this concept to the space radiator will result in an across the panel temperature gradient of essentially zero, while avoiding warpage due to thermal stresses and improving fin efficiency, which will approach 1.0. In addition, the honeycomb design offers high reliability. A radiator system of this design can be constructed in narrow, independent segments to provide redundancy for meteoroid or other forms of damage.

### 3.2.2 Manufacturing Technology Status

The technology and commercial equipment are available to construct all-welded, machine-assembled honeycomb panels. At present, such panels are constructed and formed into various shapes for use in aircraft, missile and ship frames. The honeycomb structure can be manufactured from any weldable material (excluding aluminum), up to 48 in. (1.22 m) wide in any reasonable length, with a minimum overall thickness of 0.25 in. (6.35 mm), in a variety of cell and channel sizes from 1/4 to 1/2 in. (6.35 to 12.70 mm) and shapes with different facesheet thicknesses. The basic panel is readily producible into components by cutting, stretch-forming, drawing, welding, and riveting.

For the honeycomb panels to function properly as heat pipes, the internal surfaces must be fabricated from porous materials or have porous materials attached to the internal surfaces. The structure would consist of two internally wickable faces bonded to perforated, wickable honeycomb core material. Calculations and experiments with pieceparts led to the development of machine-fabricated, wickable honeycomb subscale liquid metal test panels for thermal stress reductions in NASA Scramjet Engines.<sup>8</sup> Various test samples and prototype panels were built to evaluate alternative construction methods, to perform proof-pressure and weld integrity testing, to verify heat-pipe processing techniques, and to do performance testing. Evaluation of options resulted in final design and fabrication of 6 in. square by 1.14 in. (0.15 x 0.03 m) thick test panels, constructed entirely of stainless steel materials. Two designs for the honeycomb core were built: a foil-gauge sintered screen material, and a metal screen sintered to foil-gauge sheet material. The former design offers increased wicking capability and the

latter provides stronger structural design. Details of final panel construction (welding of sidewalls), cleaning and processing procedures, and experimentally-determined wick parameters (capillary radius,  $r_c$ , and permeability,  $K$ ) for porous core materials are reported in reference 8. Table 1 outlines current manufacturing limits on the honeycomb heat-pipe panel design.

Stainless steel and the lighter-weight titanium construction materials were both considered for panel fabrication. Stainless steel was chosen based on proven wickable core fabrication experience, and due to the availability of a much larger range of screen mesh sizes. The alternative of welding stainless steel screen core to titanium facesheets was disapproved by the panel manufacturer due to the formation of brittle welds. The facesheets are made internally wickable by sintering relatively porous 120 x 120 mesh 316 stainless steel square weave screen to 0.018 in. (0.46 mm) thick 316 stainless steel sheet.<sup>9</sup> Using multiple facesheet wick layers would increase liquid flow area, thereby improving transport capacity of the heatpipe honeycomb panel. The panel manufacturer felt that more than two layers would create excessive arcing during the weld operation, leading to a high probability of pinholes through the facesheet. Correspondingly, a minimum starting sheet thickness of 0.018 in. (0.46 mm) was recommended for high probability leak-free panels. If desired, facesheets could be made thinner after final core assembly through chem-milling. Two types of wickable honeycomb core designs were considered: 316 stainless steel sintered woven wire screen; and a 316 stainless steel screen/foil composite consisting of one layer screen sintered to 316L stainless steel foil. The sintered screen core permits liquid flow between cells because it is porous through its thickness. The screen/foil core relies solely on notches cut in the top and bottom of each honeycomb cell wall (Figure 3) for liquid flow between cells. Since the higher structural strength of the screen/foil core is not necessary for the space radiator, the sintered screen core was selected to improve transport capacity. The selected core consists of 165 x 1400 mesh sintered screen having a thickness of 0.006 inch (0.15 mm).

Alternate core ribbon designs were investigated with regard to manufacturing constraints and their implication on heat pipe capacity. Core ribbons are

TABLE 1  
MANUFACTURING LIMITS\*

Facesheet

- Longest piece before welding: 48 in. (0.64 m)

Honeycomb Panel

- Materials: stainless steel, titanium
- Longest section before welding: 120 in. (3.05 m)
- Panel width: 48 in. (0.64 m)
- Core depth: 0.25 to 2.00 in. (6.35 to 50.8 mm)
- Core ribbon thickness: 0.006 in. (0.15mm) maximum
- Cell or channel sizes: 0.25, 0.375 and 0.5 in.  
(6.35, 9.52 and 12.70 mm)
- Facesheet thickness: 0.010 to 0.030 in.  
(0.25 to 0.76 mm)

\*Dictated by materials supplier and panel manufacturer

TABLE 2  
PRELIMINARY DESIGN SUMMARY; BASIS FOR ANALYTICAL MODELING

Select design parameters

Fixed

- All-stainless steel construction
- Facesheet strip thickness: 0.018 in. (0.46 mm)
- Wire mesh laminate for core ribbon
- Overall length of panel: 120 in. (3.05 m)
- Overall panel width: 24 in. (0.60 m)

Vary

- Core ribbon depth (D): 0.25, 0.5, or 1.0 in.  
(6.35, 12.70 or 25.40 mm)
- Honeycomb size: 0.375 or 0.5 in. (9.52 or 12.70 mm),  
cell or channel
- Facesheet wick layers: 1 or 2

Optimize performance

initially punched to create desired holes or notches, are then corrugated and have their top and bottom edges folded to form mini-flanges. The honeycomb cell core is formed when the core ribbons are welded to each other at face junctions and to the facesheets and mini-flange intersections (Figure 4). The size, shape and location of honeycomb cell wall perforations are trade-offs between structural soundness and heat pipe performance. Vapor flow perforations in cell walls should be no larger than is required to keep the sonic and entrainment limits of the heat pipe from becoming overall performance limiters. Notches at the core ribbon/facesheet interface increase liquid flow due to unobstructed wick area, however, good weld consistency requires that the mini-flange itself remain intact in order that weld resistance be constant during the welding operation. Each spot weld region destroys local wicking action and thereby effectively decreases liquid flow area (inhibiting transport capacity by reducing the heat pipe wicking limitation). Typically, the panel manufacturer is intent on providing high quality structural resistance to shear and tension through close spacing of spotwelds; however, to increase liquid flow area for this application, increase in spotweld spacing should be considered. Alternately, the core can be constructed with channels placed in the direction of heat transport, which eliminates concern both for perforations (not needed) and for liquid flow pressure drop due to spotwelds.

Table 2 lists design parameters which are considered fixed as a result of preliminary design evaluation, and those which were varied during the following analytical trade-off investigation. A panel length of 120 in. (3.05m) was chosen for fabrication since this is the longest uninterrupted length which the panel manufacturer's present machine can produce. However, in order to maintain the original plan area of 20 ft<sup>2</sup> (1.86m<sup>2</sup>), the width was doubled to 24 inches (0.61m). A honeycomb cell size of 0.25 in. (6.35 mm) is not further investigated due to excessive liquid flow pressure drops at weld zones, resulting in the poorest thermal transport capacity of the several designs considered. In addition, the 0.25 in. (6.35 mm) cell size has the highest unit weight.

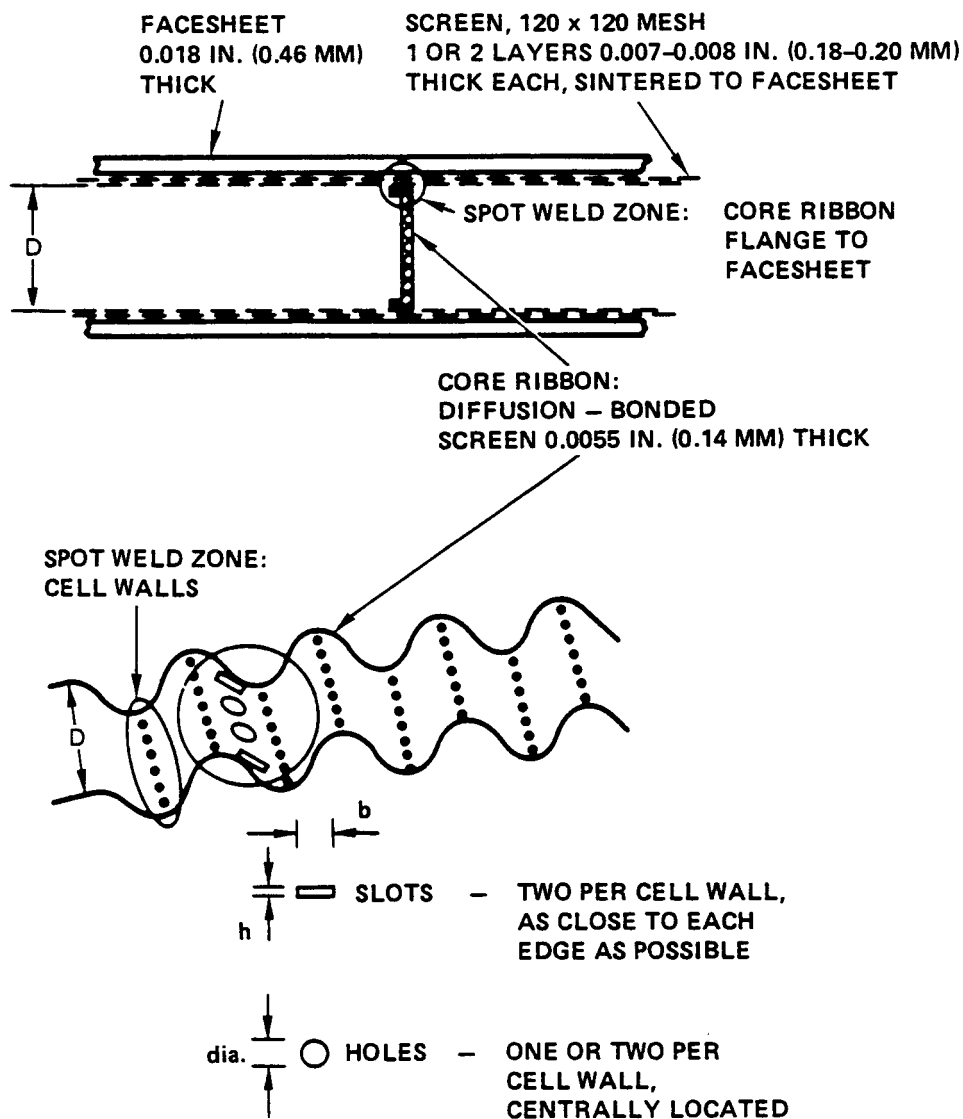


Figure 4 Core ribbon details.

### 3.2.3 Design Details and Constraints

Alleviation of face-to-face (transverse) temperature differences, hence, thermal stress problems in Scramjet wall structures at 1202°F (650°C) operating temperatures has been demonstrated.<sup>10</sup> The extension of this concept for use as a very efficient lightweight space radiator fin requires the heat flow to be in-plane rather than transverse. In-plane heat transfer dictates longer vapor flow paths through the cell walls and correspondingly longer liquid return paths along the wick-covered internal surfaces. Detailed evaluation of wick types and configurations, honeycomb cell sizes, panel thicknesses, materials, and manufacturing techniques was necessary to optimize desired panel characteristics.

As a result of experimental work reported previously,<sup>8</sup> certain design details and test data have been established, and are presently used as a baseline. The entire honeycomb panel is fabricated using an automated procedure for simultaneously resistance welding corrugated honeycomb core ribbons to each other (in the case of cells) and to both facesheets, forming 0.25, 0.375 or 0.5 in. (6.35, 9.52 or 12.70 mm) hexagonal cell or channel configurations. A sketch of the heat pipe honeycomb panel and associated component parts is shown in Figure 5.

The honeycomb panel manufacturer is machine limited to a maximum uninterrupted length of 120 inches (3.05 m). Beyond that, sections can be welded together to produce any longer length desired. The initial break in panel continuity, however, is created by weld joining of facesheet subsections. The sintered facesheet fabricator produces a maximum standard length of 48 in. (1.22 m), which dictates that honeycomb panel weld seams shall occur at least every 48 in. (Figure 6).

Since the heat flow is in the same direction as the weld seam, and since the core-ribbon crosses the welds to provide liquid communication, the detrimental effect on heat pipe performance is minimized. Conventional plasma butt-welding will produce a seam width of approximately 3/32 in. (2.38 mm). Electron beam welding can reduce the facesheet wick destruction zone to an absolute minimum, and is therefore the preferred method.



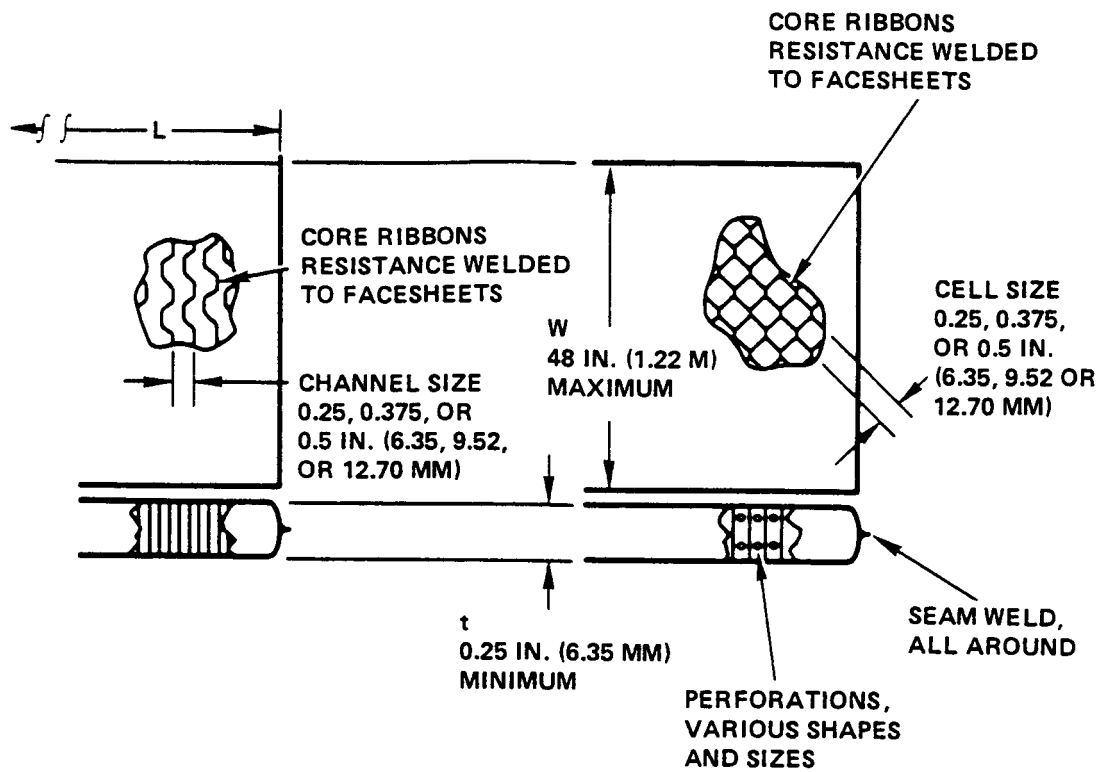


Figure 5 Sketch of heat-pipe honeycomb panel.

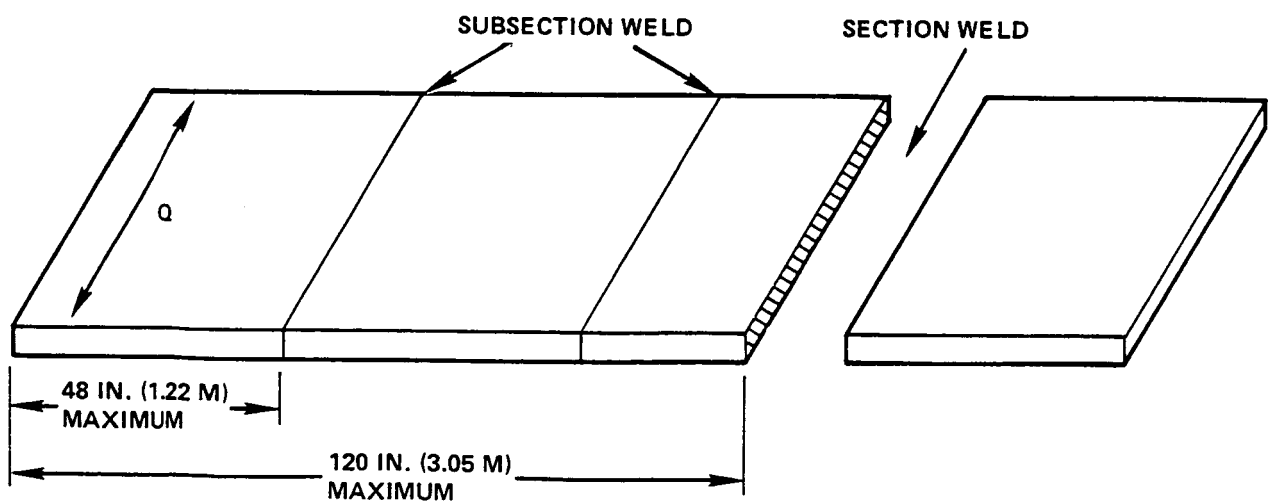


Figure 6 Panel manufacture constraints.

### 3.3 ANALYSIS

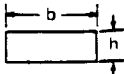

When the decision was made to double the panel width (Section 3.2.2), it was also decided to relocate the heater to a 1 inch (2.54 cm) wide strip along the centerline of the top surface. This revised condition maintains the same heat input flux of  $8.33 \text{ W/in.}^2$  ( $1.29 \text{ W/cm}^2$ ) as before, and more realistically simulates the actual space radiation fin application. Standard analytical expressions were used to calculate heat pipe performance limits for longitudinal (24 in. direction) heat transport along a 120 in. (3.05 m) length of honeycomb panel. Note, however, that the panel is symmetrical with heat input along the centerline as described above. Therefore, the analysis was performed for only one-half the actual heater and panel widths.

Critical parameters which were varied to determine the effect on maximum longitudinal thermal transport were: core ribbon depths of 0.25, 0.5 and 1.0 in. (6.35, 12.70 and 25.40 mm); 0.375 in. (9.52 mm) cell and channel and 0.5 in. (12.70 mm) cell sizes; and 1 or 2 facesheet wick layers. Transport calculations are based on methanol working fluid at the radiator operating temperature range of  $-4$  to  $149^\circ\text{F}$  ( $-20$  to  $65^\circ\text{C}$ ). Each row of adjacent cells and each channel in the longitudinal direction of thermal transport was modeled as a separate heat pipe; therefore, adjacent porous cell walls were dimensionally halved when determining wick cross-sectional liquid flow area. The multitude of liquid and vapor flow paths --the associated lengths and pressure drops -- were calculated and summed according to series or parallel path modeling. The following summary of heat pipe performance limitations contains details of the calculations.

#### Sonic and Entrainment

For the parameters selected, these are relevant only at operating temperatures lower than  $-4^\circ\text{F}$  ( $-20^\circ\text{C}$ ). Vapor flow areas are represented by openings in the direction perpendicular to intended thermal transport. Table 3 summarizes chosen parameters and assumptions used in calculating these limits.

TABLE 3  
HONEYCOMB CELL TRADE-OFF PARAMETERS

Core Depth (D)			Total X-Sect Flow Area	
			Per Face	Per Cell (X2)
0.25 in	0.065 x 0.025 in (X2)	1/16 in (X1)	0.00619 in <sup>2</sup>	0.01238 in <sup>2</sup>
0.5 in	0.065 x 0.025 in (X2)	1/8 in (X1)	0.01539	0.03078
1.0 in	0.065 x 0.025 in (X2)	1/8 in (X2)	0.02766	0.05532

Assumptions:

- Identical holes, patterns, and areas for either 0.375 or 0.5 cell sizes.
- The approximately hexagonal shape of each cell is assumed to be four-sided instead.
- The vapor flow area shall equal the total cross-sectional flow area listed in the table above.
- The equivalent radius for the slot is 0.0227 in. ( $5.8 \times 10^{-4}$  m)

TABLE 4  
DETAILS OF WICKING LIMITATIONS: DIFFERENTIAL  
PRESSURE BALANCE RELATIONSHIP

$$\Delta P_{\text{capillary}} - \Delta P_{\text{gravity}} \geq \Sigma \Delta P_{\text{vapor}} + \Sigma \Delta P_{\text{liquid}}$$

$$\Delta P_c = 2\sigma \cos \theta / r_c$$

$$\Delta P_g = \rho g (L \sin \phi + D)$$

$$\Delta P_v = \frac{8\mu_v L_{\text{eff}} Q}{\rho_v \lambda \pi (r_v^4)}$$

$$\Delta P_f = \Sigma \frac{\mu}{\rho \lambda} \frac{Q L_{\text{eff}}}{A_w K}$$

Fluid viscosity  $\sigma$ , wetting angle  $\theta$ , capillary radius  $r_c$ .

$L \sin \phi = 0.125$  in. minimum; tilt angle  $\phi$ , length  $L$   
 $D = 0.25, 0.50, \text{ or } 1.0$  in.; core depth

Assume laminar flow through area given by hydraulic radius of vapor space,  $r_v$   
 $L_{\text{eff}} = 6.0$  in.; effective length  
 Absolute vapor viscosity  $\mu_v$ , heat transfer  $Q$ , vapor density  $\rho_v$

All series flow paths:  $\Delta P_T = \Delta P_1 + \Delta P_2 + \Delta P_3 + \dots \Delta P_n$

All parallel flow paths:  $\frac{1}{\Delta P_T} = \frac{1}{\Delta P_1} + \frac{1}{\Delta P_2} + \frac{1}{\Delta P_3} + \dots + \frac{1}{\Delta P_n}$

Total pressure drop  $\Delta P_T$ , wall wick area  $A_w$ , permeability  $K$ , latent heat of vaporization  $\lambda$

Material	$K, m^2$	$r_c, m$
120x120 facesheet screen	$8.16 \times 10^{-11}$	$84.9 \times 10^{-6}$
165x1400 core screen	$7.51 \times 10^{-11}$	$23 \times 10^{-6}$

## Boiling

An evaporator heat flux of  $8.33 \text{ W/in}^2$  ( $1.29 \text{ W/cm}^2$ ) is lower than measured data of 13 to  $32 \text{ W/in}^2$  ( $2.02$  to  $4.96 \text{ W/cm}^2$ ) for methanol/stainless steel heat pipe combinations,<sup>11</sup> and is therefore non-limiting.

## Wicking

For all cases considered, capillary pumping restricts maximum heat transport. Table 4 provides details of the differential pressure balance relationship which defines maximum heat transport. Figure 7 briefly outlines the liquid mass flow ( $\dot{m}$ ) path methodology for one honeycomb cell.

The spot welded regions both at core ribbon flange to facesheet and at core ribbon cell wall interfaces were assumed to be 75 percent (25 percent porous) impervious to liquid flow. A visual inspection on remnant material revealed variation in spot weld consistency. This weld variation made it difficult to establish a percentage factor for open wick cross-sectional area. The initial

G14256

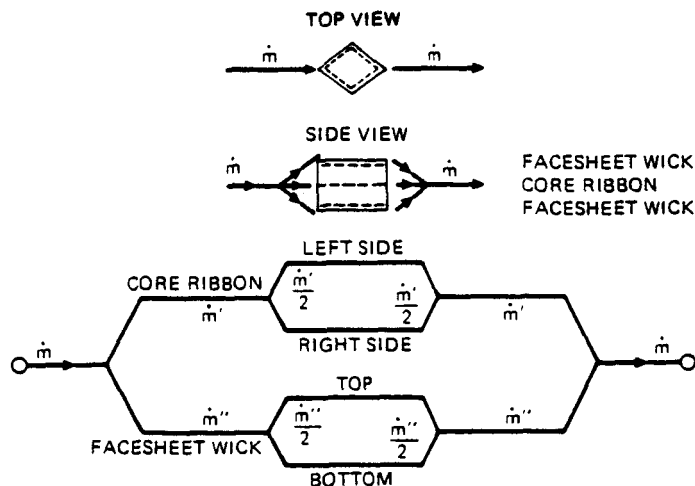


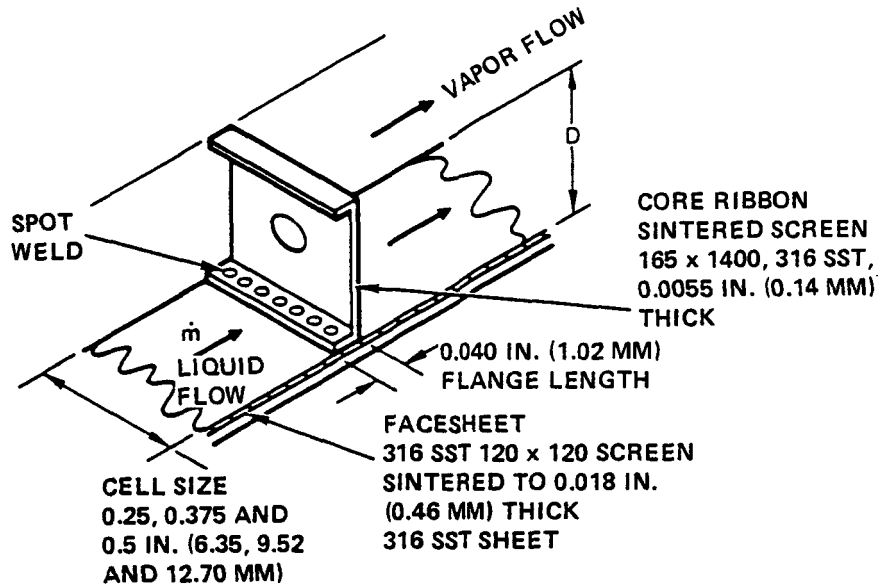
Figure 7 Liquid flow path schematic diagram: 1 cell.

estimate of 25 percent porous zone may be optimistic. Spot weld resistances in the cell configuration contribute significantly to overall liquid flow pressure drops ( $\Delta P_l$ ). Figure 8 shows a detailed schematic model of spot welded core ribbon flange to facesheet region. Predicted performance curves for several of the wickable core designs are presented in Figures 9, 10, and 11. In all cases, two layers of wick sintered to the facesheet nearly doubles the transport capacity of a single layer. Honeycomb channel design roughly triples the transport capacity of a cell design of similar size, primarily as a result of reduced pressure losses of liquid flow at weld zones and vapor flow in open channels. This analysis shows that performance is not significantly affected as honeycomb cell size varies. Relatively small increases in performance are possible as panel thickness increases from 0.25 to 1.0 in. (Figure 12).

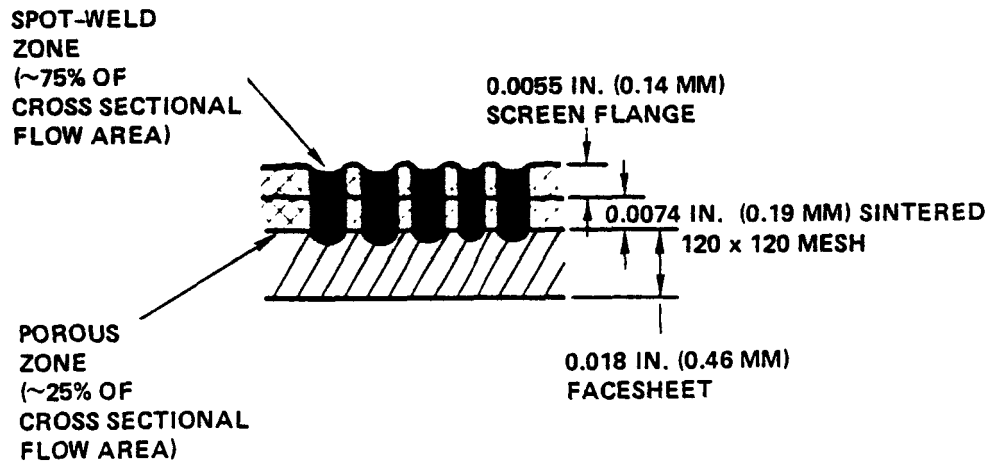
### 3.4 FINAL DESIGN

As previously stated, the initial design goal was a panel size of 240 inches x 12 inches (20 ft<sup>2</sup>-plan area). Because of manufacturing limitation, however, the length was reduced from 240 inches to 120 inches. Consequently, the width was increased from 12 inches to 24 inches in order to maintain the overall plan area of 20 ft<sup>2</sup>. The heat input zone was also relocated to the center of the panel to better simulate the intended application as a fin. Figure 13 shows a comparison between the initial and final panel design configurations.

The stated radiator power dissipation requirement throughout its operating temperature range of -4 to 149°F (-20 to 65°C) can be satisfied by any of the alternative core designs (Figures 9, 10 and 11) that were considered. The near-term objective of this program is to prove performance. A minimum transport capacity of 1000 watts (at -4°F) is predicted for a heat-pipe honeycomb cell radiator panel which measures 120 by 12 by 0.25 in. (3.05 m x 0.30 m x 6.35 mm) (Figure 10). Not requiring excess capacity, and in the interest of minimizing weight, the 0.25 in. (6.35 mm) core depth panel with a single layer of facesheet wick was chosen for construction. Moreover, the 0.5 (12.70 mm) inch cell option was selected over channels because of the previously successful honeycomb panel heat pipe construction (5, 8).



A. SCHEMATIC OF HONEYCOMB CELL WALL



B. CLOSE-UP SCHEMATIC OF CROSS-SECTIONAL FLOW AREA

Figure 8 Flange section liquid flow model.

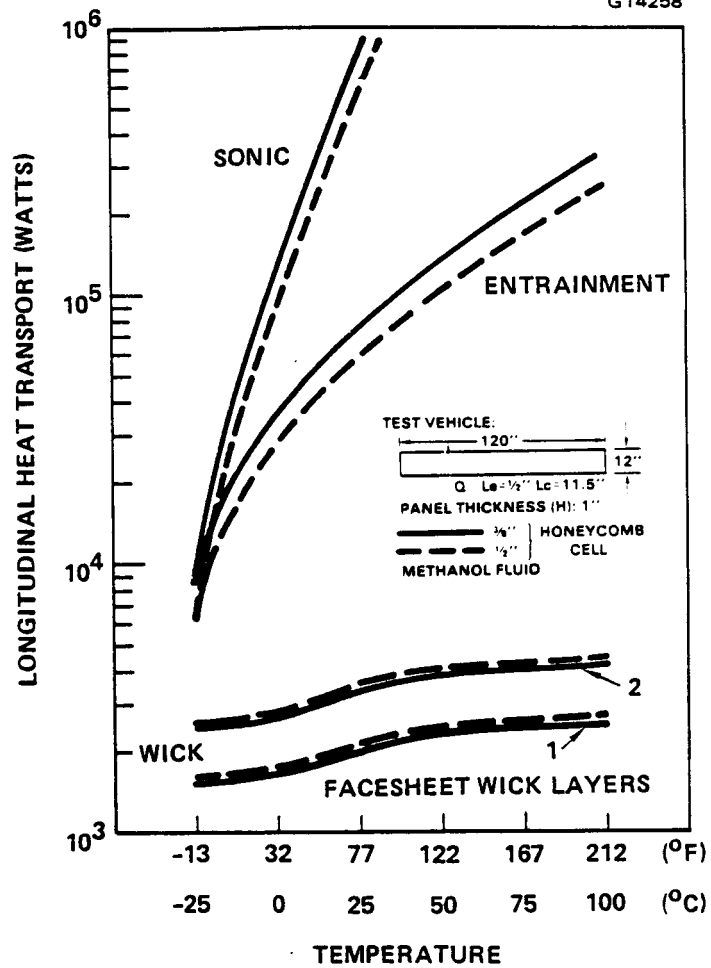


Figure 9 Performance limits vs temperature for 1 inch thick honeycomb cell panel.

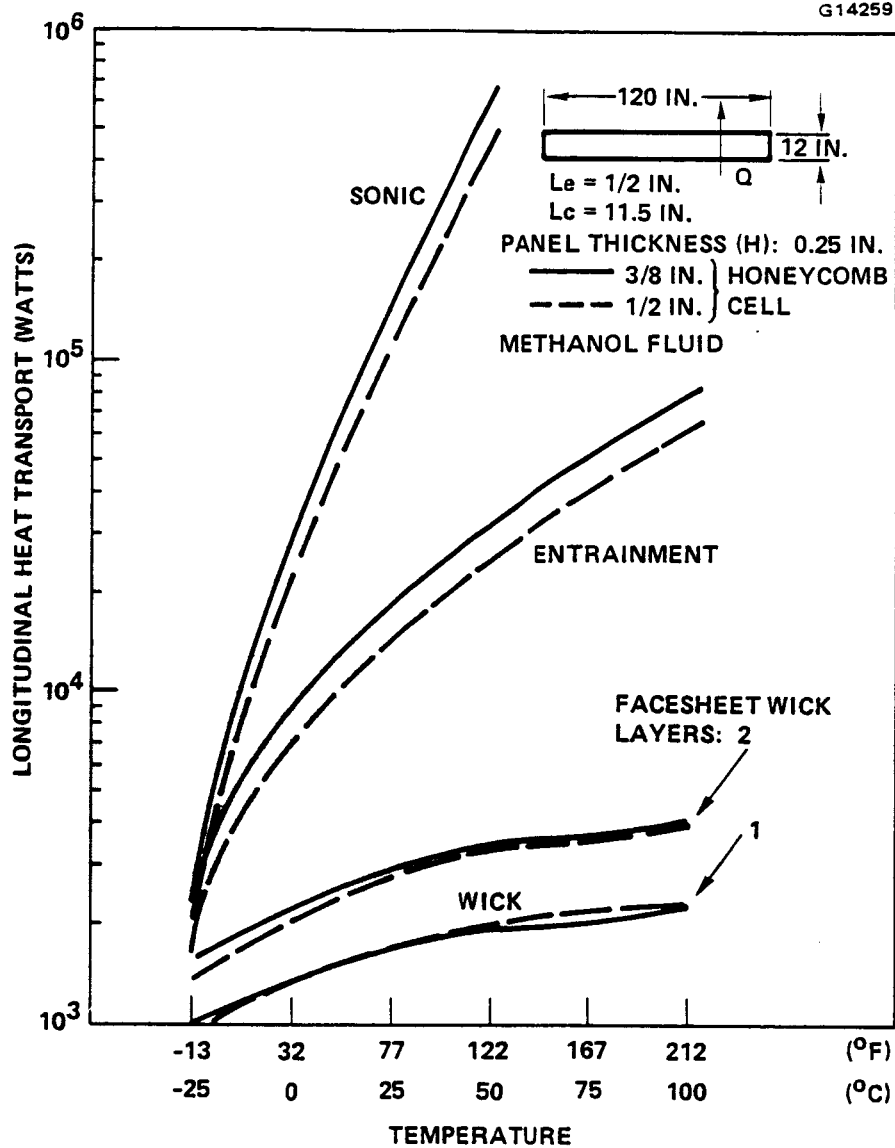


Figure 10 Performance limits vs temperature for 0.25 inch thick honeycomb cell panel.



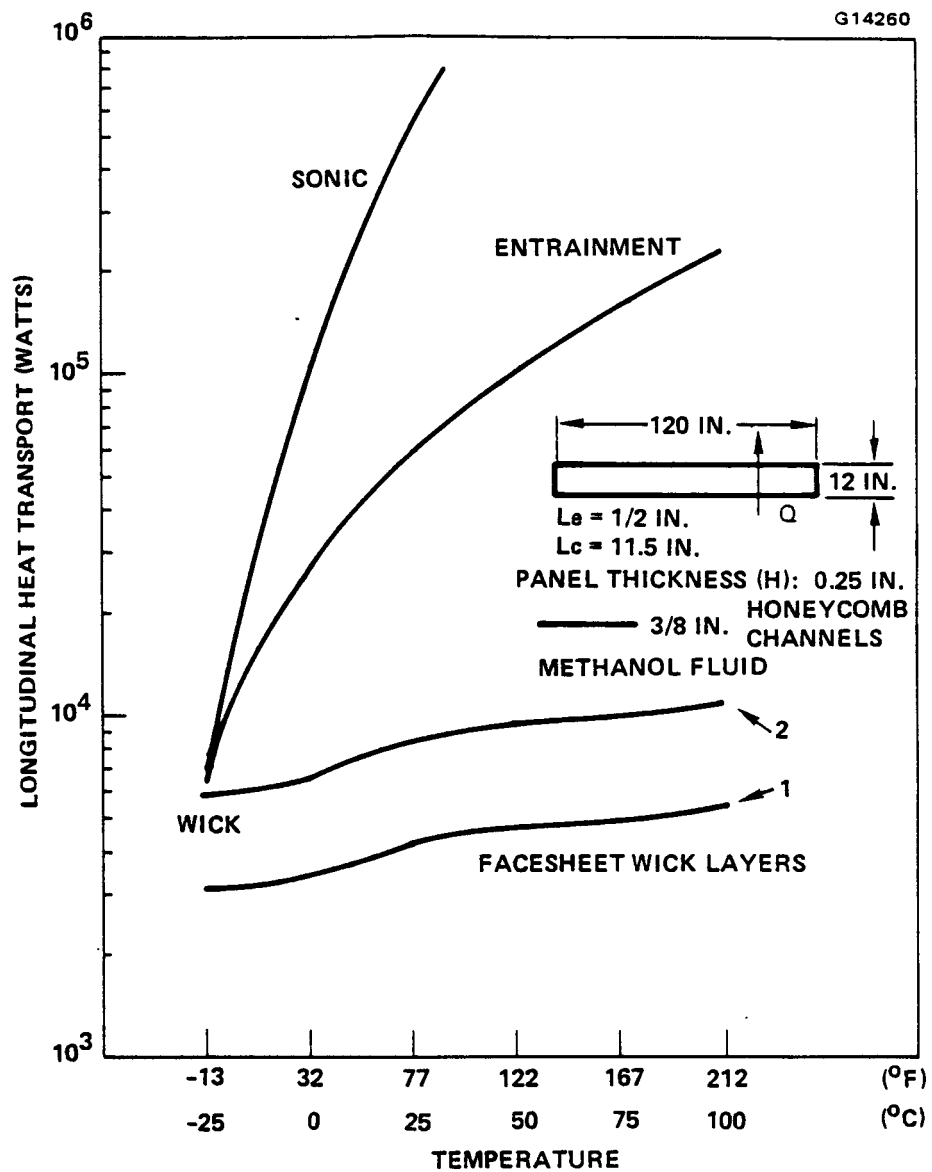


Figure 11 Performance limits vs temperature for 0.25 inch thick honeycomb channel panel.

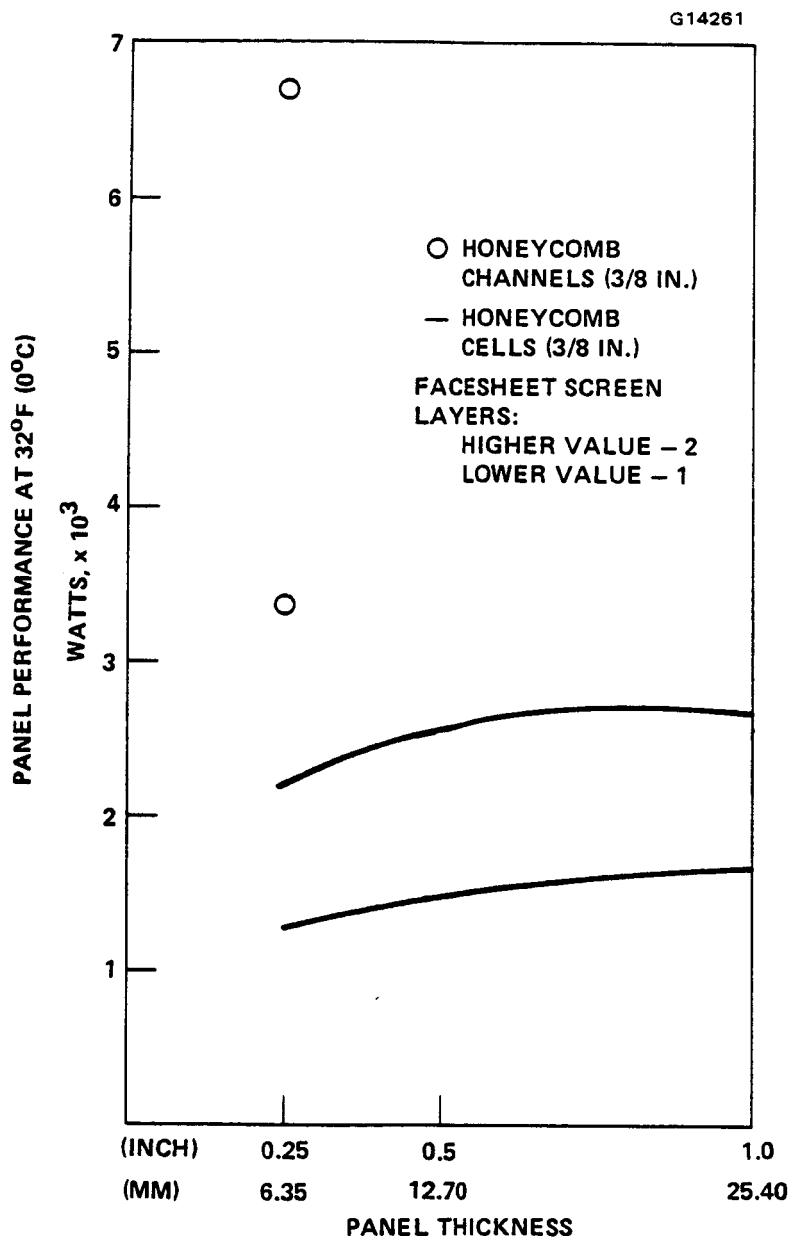
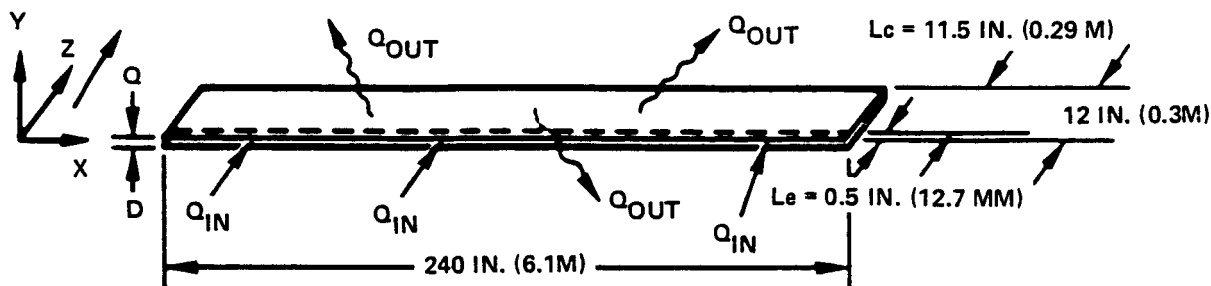


Figure 12 Panel performance vs panel thickness.

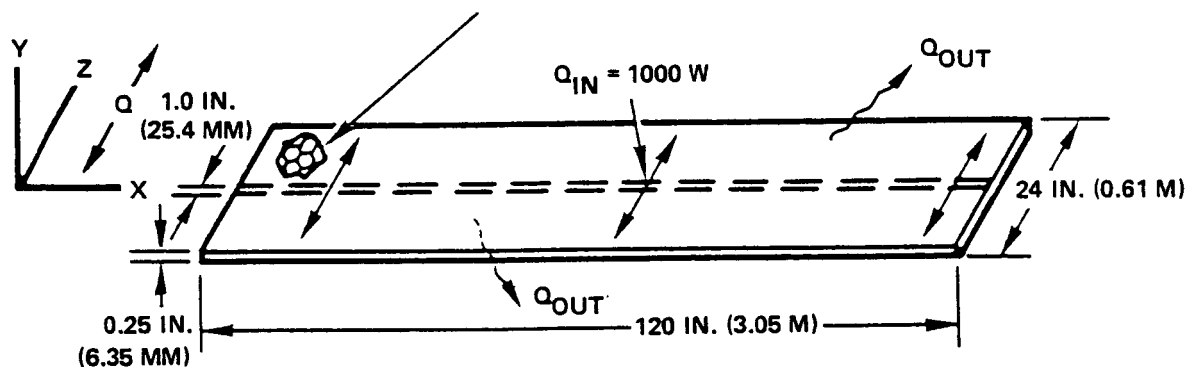
$$Q_{IN} = 1000 \text{ W HEAT INPUT AREA} = 2 (0.5 \times 120 \text{ IN.}) = 120 \text{ IN}^2 (774.19 \text{ CM}^2)$$

$$\frac{Q}{A} = \frac{1000 \text{ W}}{120 \text{ IN}^2} = 8.33 \text{ W/IN}^2 (1.29 \text{ W/CM}^2)$$



A. ORIGINAL REQUIREMENTS AND TEST CONDITIONS.

0.5 IN. (12.70 MM) HONEYCOMB CELL, 1 LAYER FACESHEET WICK,  
ALL SST CONSTRUCTION



$$Q/A = 1000 \text{ W}/(1 \text{ IN.} \times 120 \text{ IN.}) = 8.33 \text{ W/IN}^2 (1.29 \text{ W/CM}^2)$$

B. FINAL CONSTRUCTION DETAILS AND TEST CONDITIONS.

Figure 13 Comparison between initial and final panel designs.

## 4.0 FABRICATION

As the fabrication process progressed from raw materials to finished panel, several design parameters deviated from the original specification as a result of manufacturing difficulties and limitations. The following fabrication sequence describes events leading to the finished panel.

### 4.1 PIECEPARTS

#### 4.1.1 Diffusion Welded Material

As previously described, the facesheet material consists of one layer of 120 x 120 mesh 316 SST screen, diffusion bonded (sintered) to one layer of .018 in. (0.46 mm) thick 316 SST sheet. Figure 14 is a cross-section of the facesheet/sintered wick interface. The largest available stock sizes for this material are 24 x 48 in. (0.61 x 1.22 m) and 36 x 36 in. (0.91 x 0.91 m) due to vacuum furnace size limitations. To achieve a finished panel width of 24 inches (0.61 m), the panel welder requires a starting facesheet width of at least 28 inches (2 inches extra at both edges for "grabbing" the panel during the weld operation). Therefore, the 36 x 36 in. sintered stock was ordered. This facesheet material, as originally received, was unacceptable due to the presence of small, sharp depressions. The material was reworked by flattening in a rolling machine. However, it required trimming in size to 26 x 36 inch. It follows, then, that the final panel would consist of five sections joined together to create a total length of 120 inches (3.05 m); in other words, welds would occur every 26 in. rather than 48 in. as originally planned.

The core ribbon material consists of sintered 316 SST twilled-weave, wire mesh laminate (165 x 1400 mesh) which is 0.0055 in. (1.67 mm) thick. Sheets measuring 24 x 48 inches were prepared.

#### 4.1.2 Core Ribbon Fabrication

The ribbon material was cut into thin strips (48 in. long), crimped, corrugated, and then folded 90° at both 48 in. (1.22 m) edges to form mini-flanges.

E4938

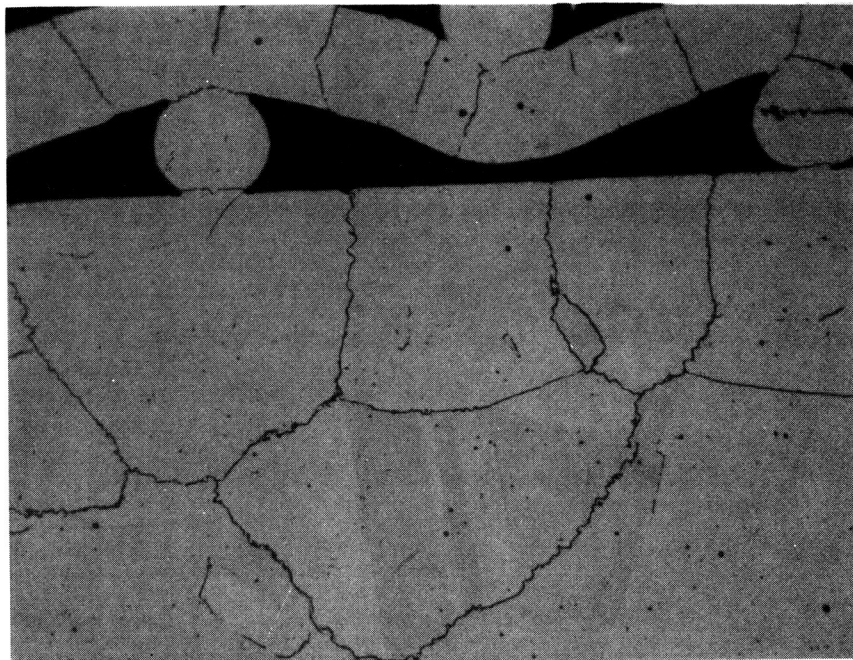


Figure 14 Cross section of facesheet/sintered wick interface (250X).

E4939

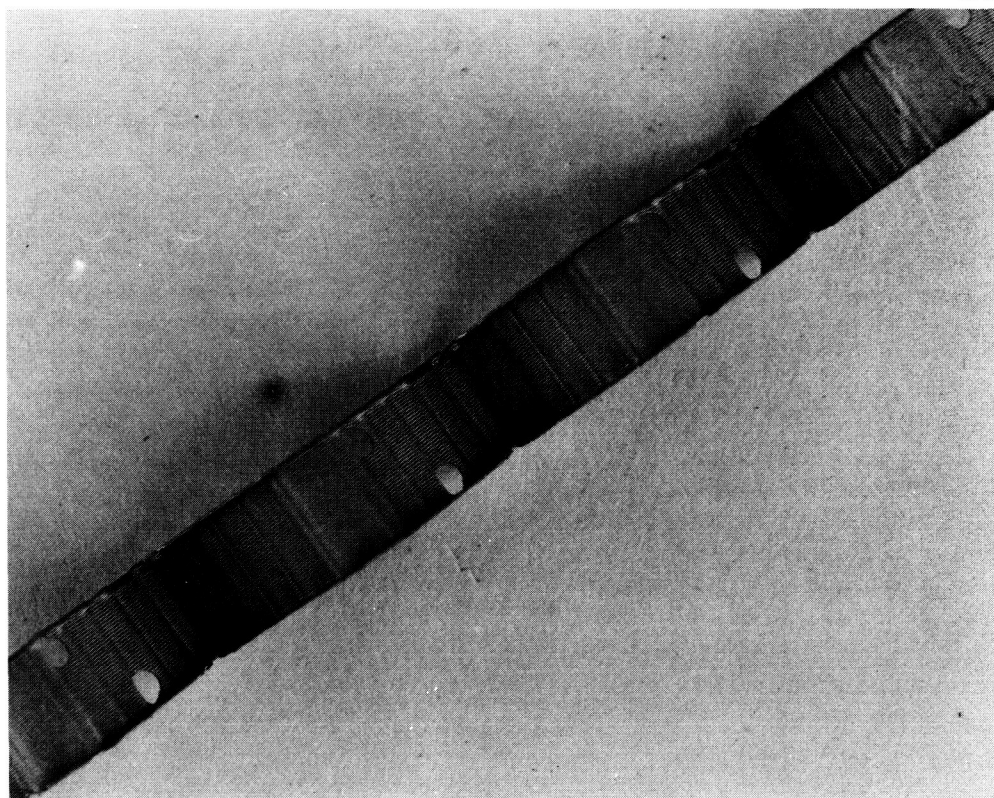


Figure 15 Core ribbon material after crimping.

Holes (perforations) were punched into the ribbon with small dies. Constraints on hole placement are related to cracking and buckling of the ribbon during subsequent panel weld operations. After some experimentation, the panel welder settled on the inclusion of two 1/16 in. (1.59 mm) diameter holes which were located very near the mini-flanges at the top and bottom of every second cell face (vapor flow area through the honeycomb cells is the summed open area from two faces per cell). A photograph (Figure 15) of the finished core ribbon shows the holes punched on alternating cell walls. However, the actual vapor flow area was only 75 percent of that originally desired. Also, vapor flow was constrained to a diagonal direction through the panel, or a 41 percent increase in travel length from the straight direction.

Liquid transport is affected by the location and spacing of spot welds in its flow path. An increase of mini-flange to facesheet spot weld spacing was requested. However the actual extent of this increase is unclear. Upon close examination of a finished panel specimen, variance in spotweld consistency makes it difficult to establish a percentage factor for "open" wick cross sectional area. The initial estimate of 25 percent porous zone (see Section 3.3, under Wicking) may be optimistic. Thermal transport capacity predictions are sensitive to this available wicking flow area. However, spot welds at core ribbon cell wall interfaces (see Figure 4) were eliminated entirely (as requested) and this should increase transport capacity contribution of the core wick.

#### 4.1.3 Panel Facesheet Joining

Electron beam welding of the facesheet sections was originally planned, but due to cost and time constraints, the panel fabricator elected to use butt-weld (GTAW), shown in Figure 16. Four butt welds of this type were used for welding five facesheet sections into an overall length of 120 inches (3.05 m). Note that these welds are in the transverse direction parallel to the liquid flow path. Moreover, the core ribbon material crosses these welds to provide liquid flow communication.

E4940

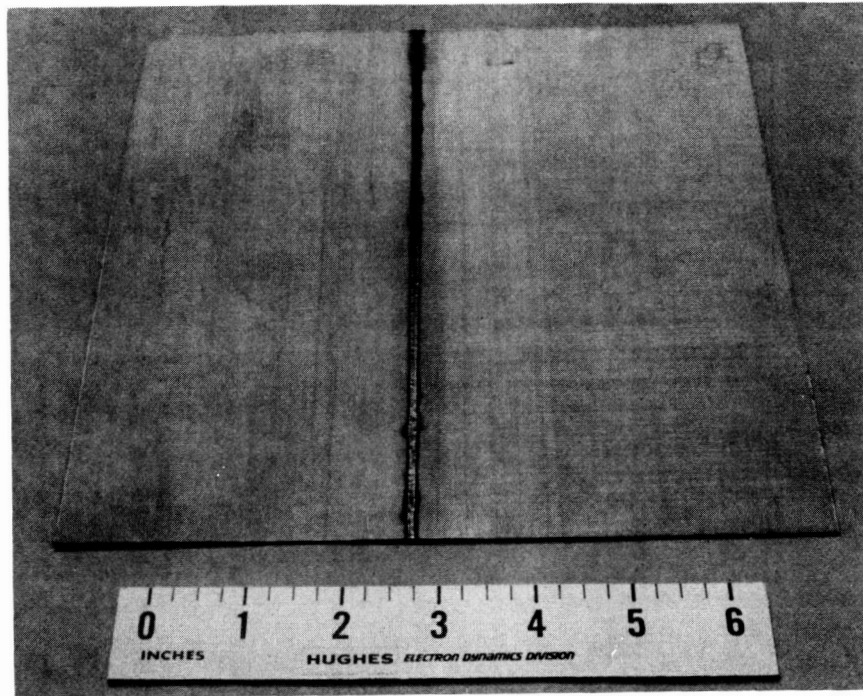


Figure 16 Butt welded face sheet sample showing  
sintered screen wick.

E4941

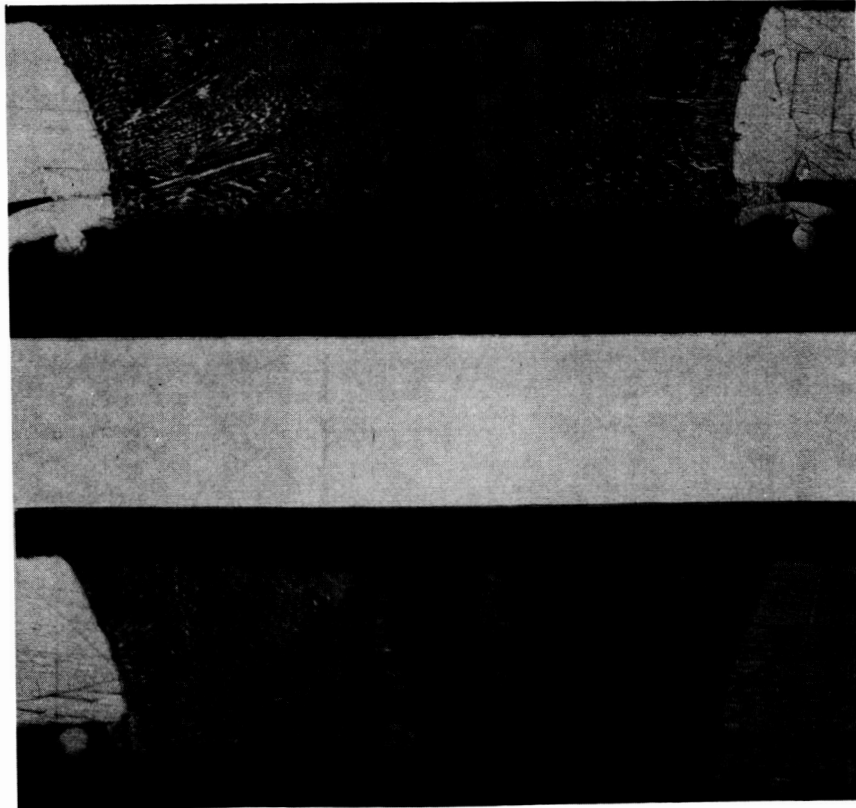


Figure 17 Butt welded (GTAW) face sheets for heat pipe.

Metallurgical cross-sections of the butt-welded face-sheet samples are shown in Figure 17. These cross-sections were provided by the honeycomb panel manufacturer, Astech<sup>R</sup>, Division of TRE Corp., Santa Ana, California.

#### 4.2 HONEYCOMB PANEL

Figure 18 is a close-up photograph of the internal honeycomb structure with one facesheet removed. The sintered core material (ribbons), perforated holes for vapor and liquid communication among the cells, and facesheet wick sintered to the facesheet material can be seen in this photograph. Spotwelds for attaching the core ribbon to the facesheets and a facesheet butt weld are also visible.

After fabrication and trimming of the honeycomb panel material to size (24 in. x 120 in.), a rolled edge was formed, completely encircling the panel. The edge was butt fusion (GTAW) welded all-around to produce a leak-tight seal (Figure 19). A 1/4 inch diameter hole was drilled at the center of one short (24 in.) edge and a 1/4 inch (6.35 mm) diameter x 12 inch (0.30 m) length fill tube was welded in place. This technique resulted in a single edge weld rather than two welds plus additional piece-parts for the edges as originally envisioned. The completed panel is shown in Figure 19. The final leak test consisted of internally pressurizing the panel to 5 psig using helium, and verifying leak tightness with a high speed sniffer probe attached to a Veeco<sup>R</sup> mass spectrometer.

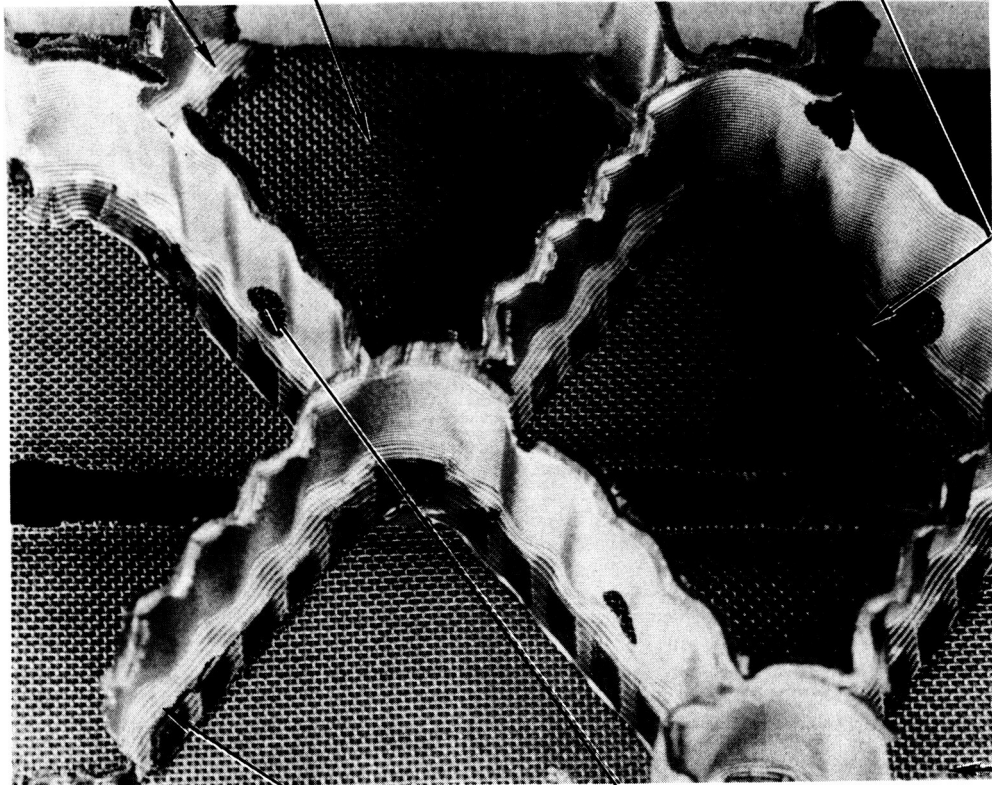


E4942

CORE RIBBON: 165 X 1400 MESH  
SINTERED LAMINATE

FACESHEET: 1 LAYER SINTERED  
120 X 120 MESH

DIRECTION  
(FLOW  
RESTRICTED  
45° TO  
DIRECTION  
OF HEAT  
TRANSPORT)



FACESHEET  
BUTT WELD

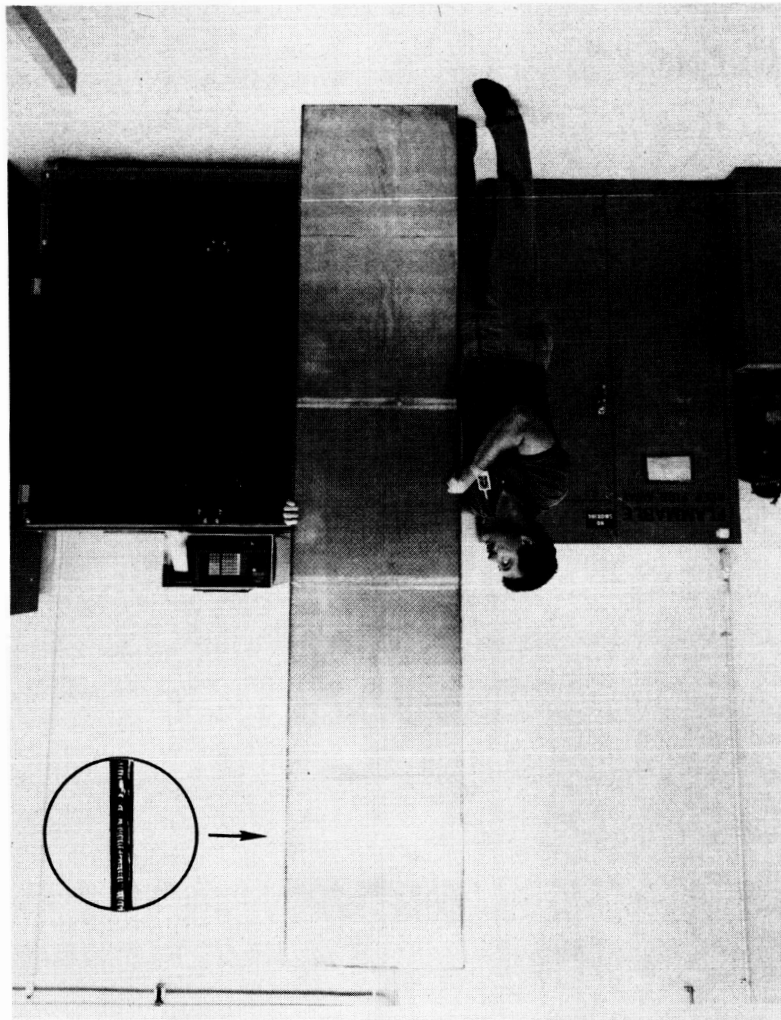
FACESHEET  
SPOT WELD

PUNCHED  
VAPOR  
HOLE

DIRECTION  
OF  
INTENDED  
HEAT  
TRANSPORT

Figure 18 Close-up of internal honeycomb structure.

Figure 19 Completed honeycomb panel.



E4943

ORIGINAL PAGE IS  
OF POOR QUALITY

## 5.0 TEST PERFORMANCE

Preliminary performance testing and checkout of the honeycomb panel heat pipe were conducted in laboratory ambient air. For testing over the temperature range of  $-4$  to  $149^{\circ}\text{F}$  ( $-20^{\circ}\text{C}$  to  $65^{\circ}\text{C}$ ), however, the panel was installed in a special test station. The test station, methods, and heat transport performance test results are described in the following paragraphs.

### 5.1 TEST SETUP

Figure 20 is a photograph of the test station designed for testing the honeycomb panel performance over the temperature range  $-4$  to  $149^{\circ}\text{F}$  ( $-20^{\circ}\text{C}$  to  $65^{\circ}\text{C}$ ). Referring to the sketch in Figure 21, it can be seen that the heat sink is provided by six 8 inch (0.20 m) wide flanged aluminum extrusions with 1 inch (25.4 mm) diameter liquid nitrogen ( $\text{LN}_2$ ) coolant passages. Three extrusions are placed above the test panel and three below for heat rejection from both sides of the panel. The test panel is centered approximately 3 inches (76.2 mm) from the flanged surfaces of the heat sinks, using a total of eight adjustable plexiglass support pegs. The test setup was enclosed in a 132 inch long x 30 inch wide X 24 inch (3.35 x 0.76 x 0.61 m) high plexiglass chamber. Note that this is not a vacuum chamber, and heat transfer from the heat pipe to the heat sink is by radiation, conduction, and natural convection through the surrounding air.

Thirty chromel-constantan (Type E) thermocouples were spot-welded directly to the panel surface at the locations shown in Figure 22. Thermocouples on the bottom surface are placed directly underneath the top ones. Note, however, that there are no thermocouples underneath the four circled ones (Figure 23). The reason for this is that a thirty channel strip chart recorder was selected for recording the data. Since there are no edge effects associated with these locations, it is felt that the top thermocouples are sufficient.

Heat input was provided by four strips of Clayborne Labs heater tape (E-16-2) wired in parallel. For initial testing the heat input zone was a one inch (25.4 mm) wide strip running the entire length of the panel (120 inches), as shown in Figure 22. This approach simulates the honeycomb panel being used as

ORIGINAL PAGE IS  
OF POOR QUALITY

E4944

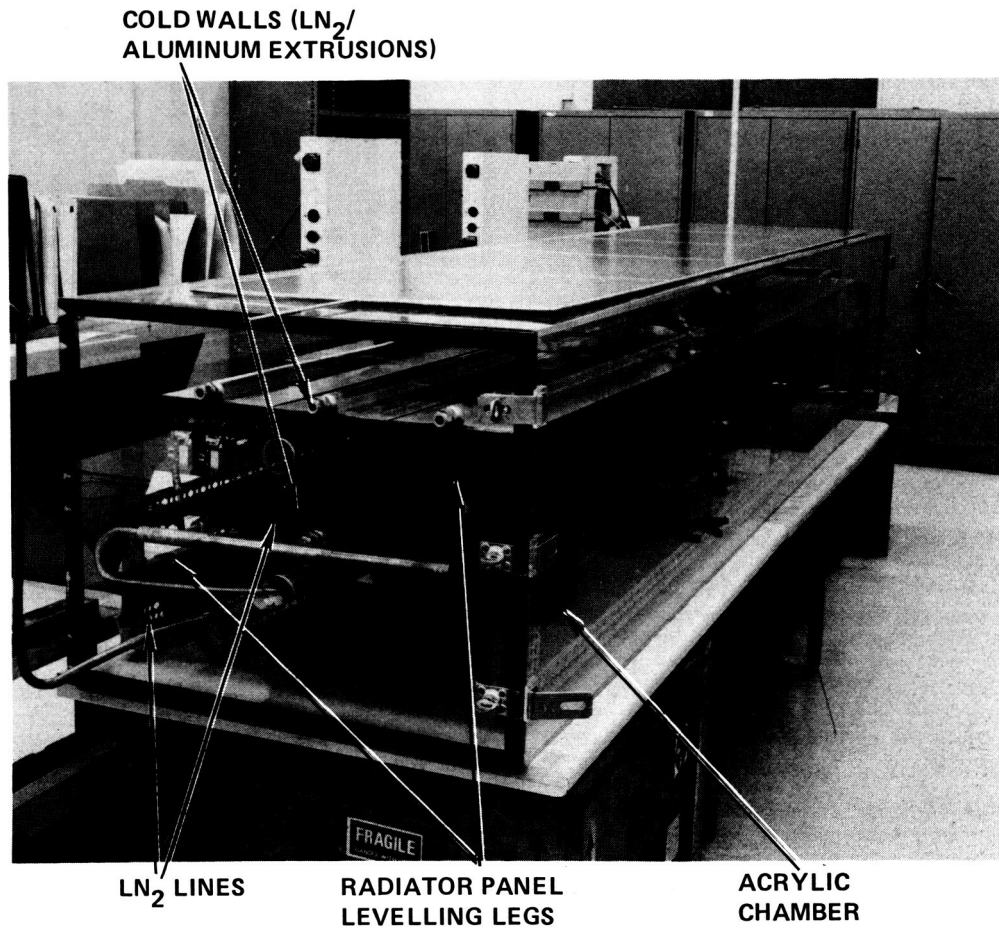


Figure 20 Performance test set-up.

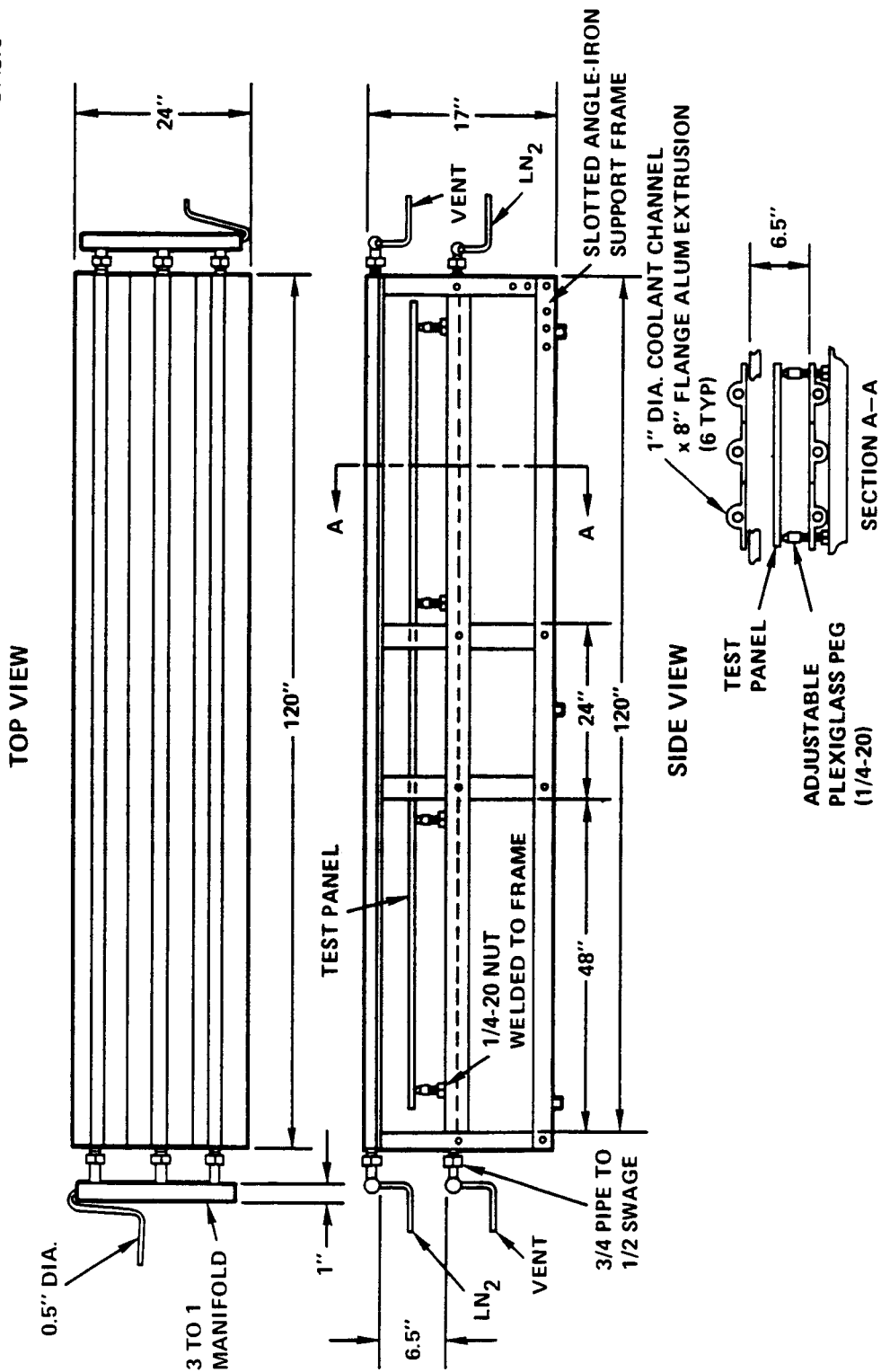
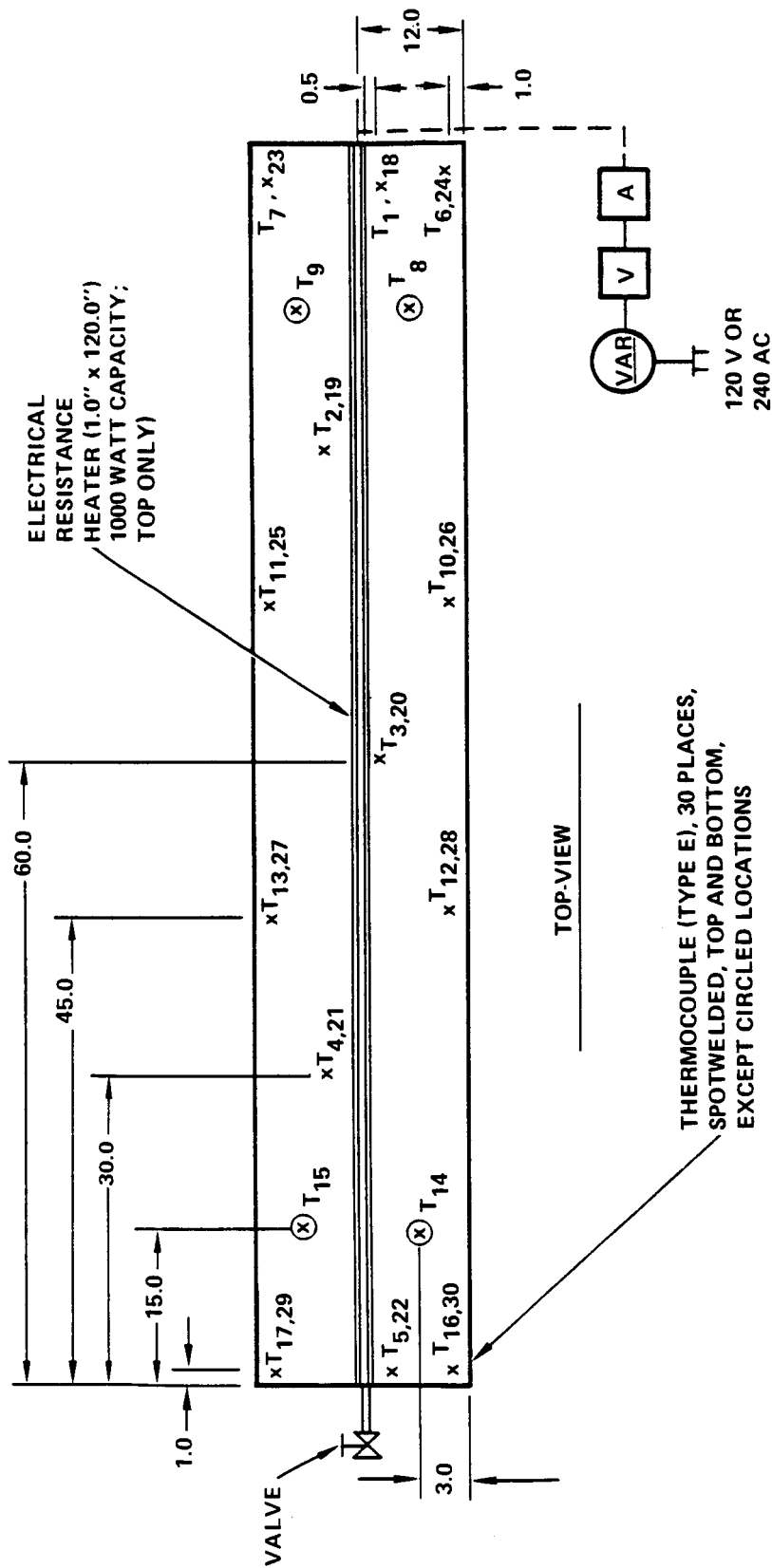


Figure 21 Schematic diagram of test station.



## NOTES:

1. CIRCLED THERMOCOUPLES ON TOP ONLY
2.  $T_{a,b}$ ; WHERE a = TOP TC NO. AND b = BOTTOM TC NO.
3. INSTRUMENTATION IS SYMMETRICAL, EXCEPT AS NOTED
4. DIMENSIONS IN INCHES

Figure 22 Honeycomb panel performance test instrumentation.

a high efficiency radiator fin in conjunction with a high capacity axial transport heat pipe or coolant loop.

## 5.2 PROCESSING PROCEDURES

The test panel was received at Hughes on November 21, 1983. The panel was subjected to a leak test by internally pressurizing the panel to 5 psig using helium, and checking for leaks with a high speed sniffer probe attached to a Veeco<sup>TR</sup> mass spectrometer leak detector. No leakage was detected.

Following this leak test, the panel was vacuum baked at a temperature of approximately 1490°F (650°C) for a period of 261 hours. Electrical resistance heater tapes were bonded to the external surfaces to provide an elevated temperature during bakeout. The panel outlet pressure was on the order of  $10^{-5}$  torr during the entire bakeout period.

The panel was then processed with 1.14 lb<sub>m</sub> (0.518 kg) of methanol by vacuum distilling the methanol into an evacuated stainless steel cylinder. This cylinder was connected to a valve attached to the previously evacuated panel, and the methanol was drained into the panel under vacuum conditions. The appropriate fill was determined experimentally by weighing a small sample of residual honeycomb material before and after saturating the wicks with methanol. This approach provided the amount of methanol per unit of panel area. Even though the methanol in the charging cylinder was degassed prior to filling, the panel was also subjected to the degassing procedure to provide assurance against the possibility of introducing gas during the transfer of methanol. The degassing was accomplished by placing a 3-inch thick layer of open cell polyurethane foam underneath and on top of the panel, and cooling by pouring liquid nitrogen onto the top layer. When the panel was sufficiently cooled (<-40°F) the fill valve was opened to vacuum to vent the gases.

### 5.3 TEST RESULTS

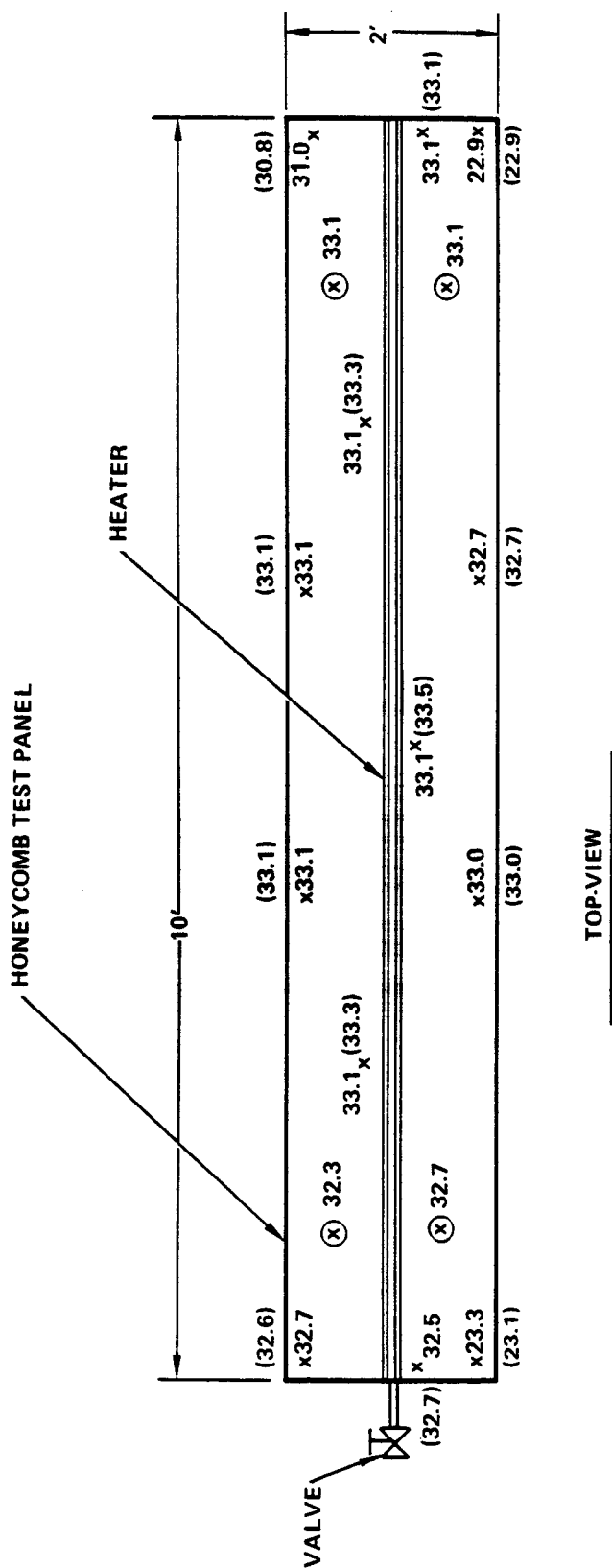
#### 5.3.1 Ambient Air Testing

As mentioned above, preliminary checkout of the honeycomb panel heat pipe was conducted in laboratory ambient air. The panel was instrumented, as shown in Figure 22, and was level to within  $\pm 1/8$  inch ( $\pm 3.18$  mm) by using a large carpenter's level and by adjusting the screw-thread plexiglass support legs. An initial power of 180 watts was applied to the heater with the panel on the bench. The resulting steady state temperature distribution is given in Figure 23. Note that the heater is on the top surface only. The entire active surface of the panel is isothermal with  $\pm 1.8^{\circ}\text{F}$  ( $\pm 1^{\circ}\text{C}$ ). Next the power was increased to 280 watts and 400 watts. Figure 24 is a strip chart recording showing all 30 temperature traces at 400 watts. At 570 watts there was evidence of hot spots (local dryout) in the area of thermocouple numbers 2 and 19.

In both Figure 23 and Figure 24 it can be seen that there are two cold corners on the panel, as indicated by thermocouple numbers 6, 16, 24 and 30. These inactive zones were approximately 6 inches by 6 inches (0.15 x 0.15 m) at each corner. Since both of these corners were on the same longitudinal edge, that side was elevated to distinguish possible liquid slugging from gas. With sufficient time, the thermocouples (6, 24) on the corner opposite the process tube and valve fell in line with the others, leaving only one inactive area (16, 30), as shown in Figure 25. This indicates that the corner identified as 6, 24 was observed to be cold due to the accumulation of liquid in that area, while the other corner must be either noncondensable gas or closed off from the remainder of the heat pipe.

Acting on the assumption that the other corner was due to gas, the heat pipe was connected to the vacuum system for a second degassing attempt. This resulted in no observable change in performance. Next, heaters were bonded in each corner near the process tube and insulated. These heaters were allowed to operate approximately eighteen hours (overnight) in an attempt to displace gas and disperse it to another location in the panel. The centerline heater was started while the corner heaters were still on. Then, when this heater



NOTES:

1. TEMPERATURES IN °C
2. NUMBERS IN PARENTHESES INDICATE BOTTOM SURFACE TEMPERATURE
3. SINK TEMPERATURE 20° TO 25°C
4. LEVEL ( $\pm 1/8$  in.)

Figure 23 Performance test temperature distribution at 180 watts heat input.

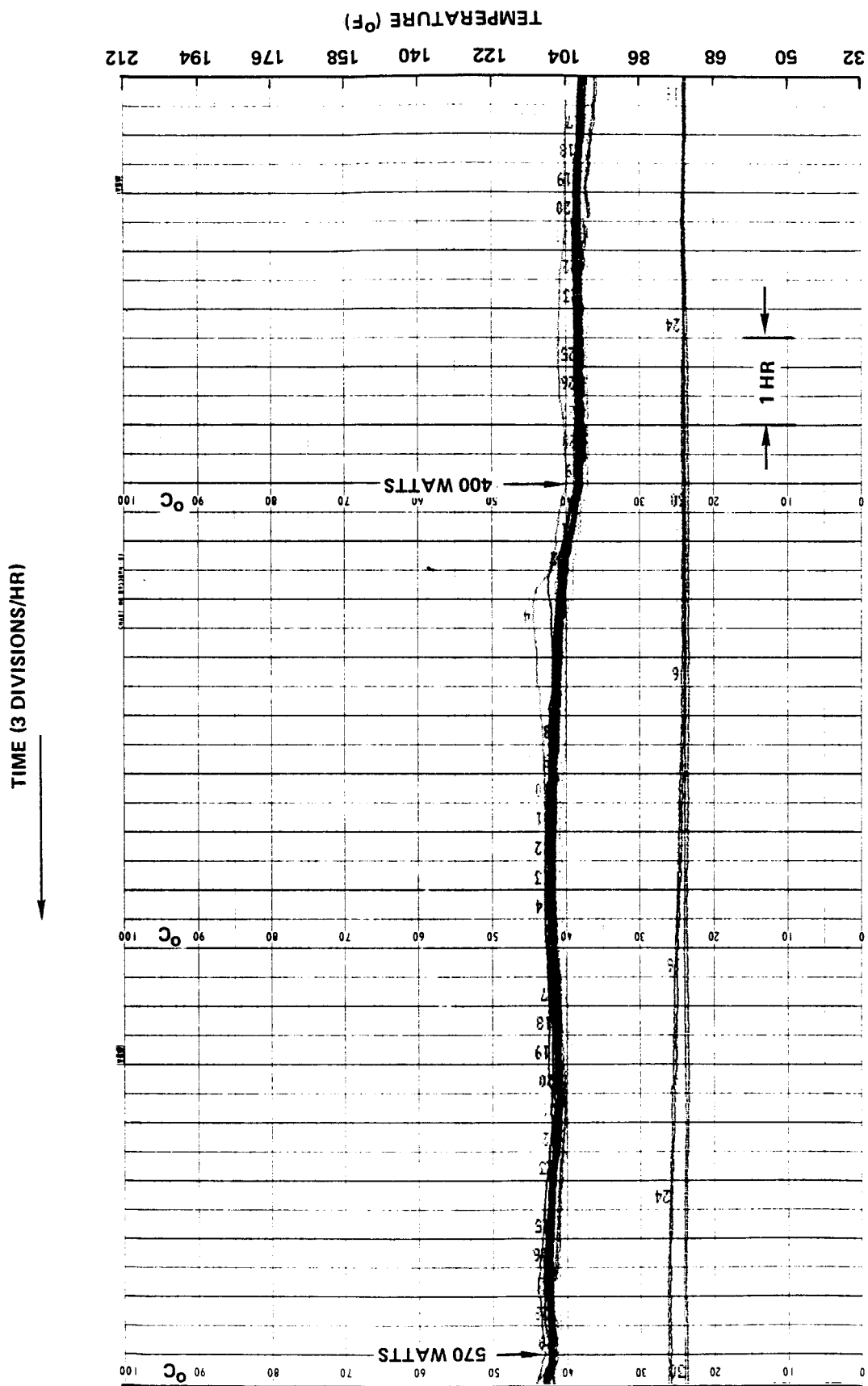
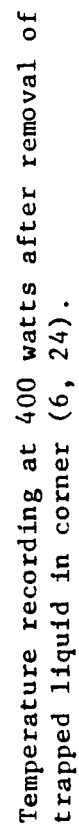


Figure 24 Strip chart temperature recording at 400 watts.

TEMPERATURE (°F)



was increased to 300 watts, the insulation was removed and the corner heaters were turned off. Thermocouple numbers 16 and 30 immediately began a steady drop-off to return to their original position. For these reasons it was concluded that this was a "dead corner." It behaved as though no fluid occupied this area. At this point, it was decided to proceed with testing over the temperature range  $-4$  to  $149^{\circ}\text{F}$  ( $-20^{\circ}\text{C}$  to  $65^{\circ}\text{C}$ ).

### 5.3.2 Performance Testing Over the Temperature Range $-4$ to $149^{\circ}\text{F}$ ( $-20^{\circ}\text{C}$ to $65^{\circ}\text{C}$ )

The honeycomb panel heat pipe was installed in the test chamber (Figures 20 and 21), and an initial checkout was performed. This was to verify results consistent with bench testing.

The cold test was performed first. First only the lower cold wall was turned on. With 100 watts input to the panel, the temperature was lowered approximately  $27^{\circ}\text{F}$  ( $15^{\circ}\text{C}$ ) in 1 hour. When the lower cold wall was turned off and the upper one turned on, the panel was cooled an additional  $39.6^{\circ}\text{F}$  ( $22^{\circ}\text{C}$ ) in one-half hour. This translates into a cooling rate of three times higher than that observed with the lower cold wall. This indicates that natural convection coupling between the panel and the upper cold wall was significantly higher than for the lower cold wall, as would be expected. The steady state temperature results are tabulated in Table 5, and the corresponding strip chart recording is given in Figure 26. When the power was increased to 120 watts, a dry-out was observed.

For elevated temperature operation, the upper and lower cold walls were not used. The interior air temperature of the chamber was heated by ducting the exhaust air from an environmental chamber into the test chamber. A small fan was provided inside to distribute the air uniformly. Steady state temperatures for a nominal temperature of  $149^{\circ}\text{F}$  ( $65^{\circ}\text{C}$ ) and a power of 500 watts are tabulated in Table 6. The corresponding strip chart recording is shown in Figure 27. A dry-out was observed at 550 watts.

TABLE 5  
HONEYCOMB PANEL TEMPERATURE  
DISTRIBUTION AT 100 WATTS (COLD TEST)

Thermocouple No.*	Temperature		Thermocouple No.*	Temperature	
	°F	°C		°F	°C
1	4.6	-15.2	16	5.2	-14.9
2	8.6	-13.0	17	8.6	-13.0
3	11.8	-11.2	18	5.0	-15.0
4	8.8	-12.9	19	8.6	-13.0
5	8.2	-13.2	20	12.2	-11.0
6	4.1	-15.5	21	9.0	-12.8
7	6.1	-14.6	22	8.2	-13.2
8	4.8	-15.1	23	5.9	-14.5
9	7.7	-13.5	24	Open	Open
10	9.5	-12.5	25	11.4	-11.4
11	11.6	-11.3	26	9.5	-12.5
12	9.5	-12.5	27	11.1	-11.6
13	11.3	-11.5	28	9.3	-12.6
14	8.1	-13.3	29	8.4	-13.1
15	8.6	-13.0	30	6.3	-14.3

\*See Figure 22 for thermocouple locations.

TABLE 6  
HONEYCOMB PANEL TEMPERATURE  
DISTRIBUTION AT 500 WATTS (ELEVATED TEMPERATURE)

Thermocouple No.	Temperature		Thermocouple No.	Temperature	
	°F	°C		°F	°C
1	149.5	65.3	16	103.6	39.8
2	149.9	65.5	17	149.0	65.0
3	156.4	69.1	18	148.8	64.9
4	149.5	65.3	19	150.1	65.6
5	149.0	65.0	20	149.7	65.4
6	148.1	64.5	21	151.0	66.1
7	149.5	65.3	22	149.2	65.1
8	149.5	65.3	23	149.0	65.0
9	149.5	65.3	24	150.1	64.6
10	149.5	65.2	25	149.5	65.3
11	149.4	65.2	26	149.4	65.2
12	149.2	65.1	27	149.2	65.1
13	149.5	65.3	28	149.2	65.1
14	149.4	65.2	29	148.6	64.8
15	149.4	65.2	30	102.6	39.2

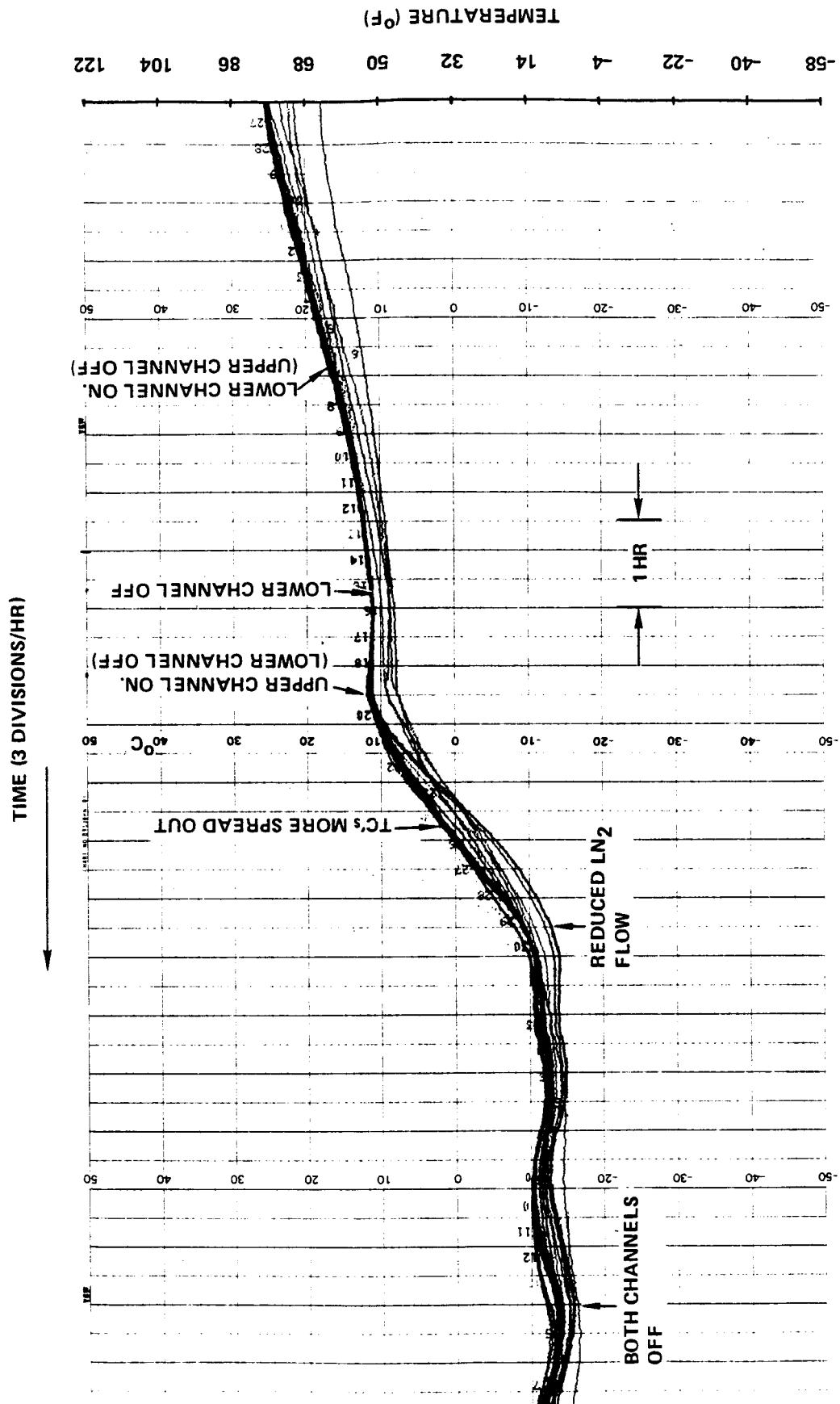


Figure 26 Temperature recording at 100 watts (Cold Test).

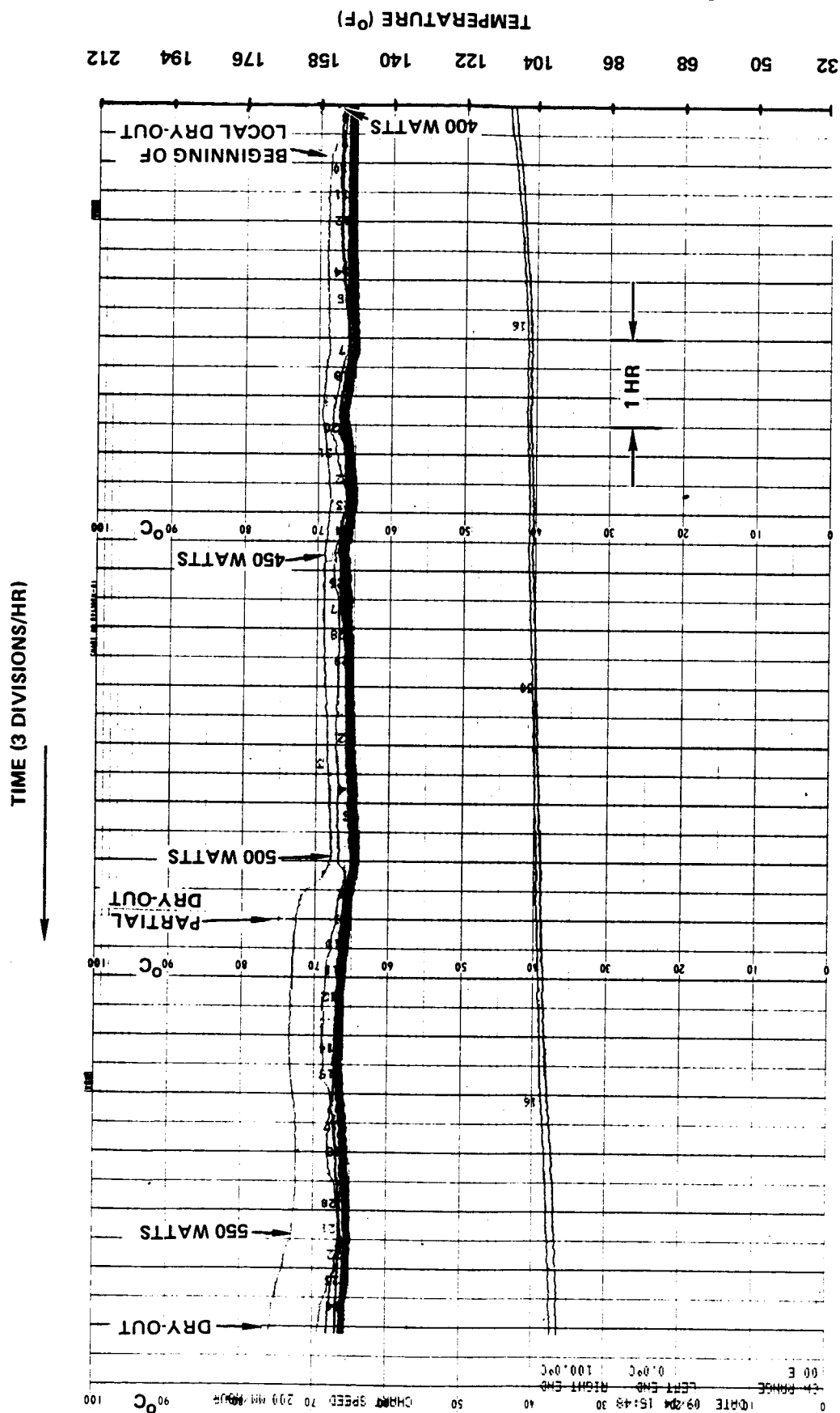


Figure 27 Temperature recording at 500 watts (Elevated Temperature).

### 5.3.3 Liquid Fill Test

After completion of the low and high temperature performance testing the panel was removed from the test chamber and connected to the process station. An additional 50 grams of methanol were added to the panel in order to start the liquid fill test. This corresponds to a 10 percent increase in the liquid fill.

The methanol was added to the panel in a manner identical to the initial processing (Section 5.2), except the panel was not evacuated prior to filling. Even though the methanol in the charging cylinder was degassed prior to filling, the panel was also subjected to the degassing procedure described in Section 5.2 to provide assurance against the possibility of introducing gas during the transfer of methanol.

The honeycomb test panel was then removed from the process station and installed in the test chamber. Upon initial application of 100 watts to the heater, a dry-out condition was observed for the central portion of the panel. This is an indication that the working fluid does not readily redistribute itself inside the panel, and there may be excessive welding of the core ribbon to the panel facesheets.

Figure 28 shows the results for the 110 percent fill test. Although there was still a local area near the center of the heater that was  $8.1^{\circ}\text{F}$  ( $4.5^{\circ}\text{C}$ ) warmer than the remainder of the active panel surface, there was no evidence of excess liquid. For this reason, it was decided to increase the methanol fill by 10 percent again.

This time the panel was tested on the bench in order to facilitate the detection of excess liquid by tilting in various directions. When the methanol fill was increased to 120 percent, the performance was essentially the same as at 100 percent and 110 percent; i.e. no evidence of excess liquid at 400 watts heat input. This shows that the panel was relatively insensitive to an underfill. The fill was then increased by 10 percent again to 130 percent.



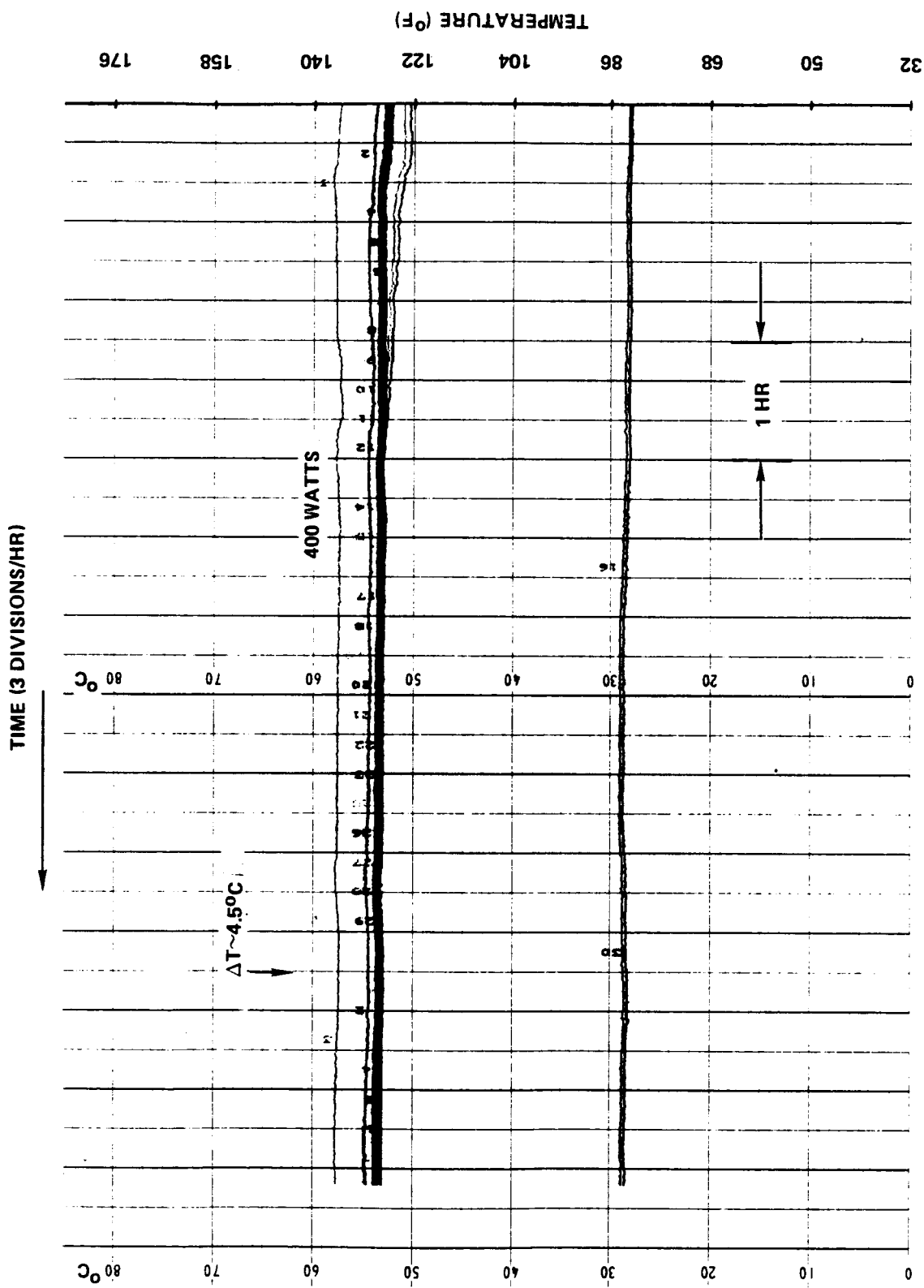


Figure 28 Temperature recording at 400 watts (110% fill).

At this time it was decided to perform a maximum power test to determine if the additional fill had any effect on the heat transport capacity. As shown by the results in Figure 29, the maximum power increased to 600 watts with only a  $+2.7^{\circ}\text{F}$  ( $+1.5^{\circ}\text{C}$ )  $\Delta T$  over the entire active surface of the panel. At 700 watts the  $\Delta T$  increased to  $19.8^{\circ}\text{F}$  ( $11^{\circ}\text{C}$ ) and this was considered to be a dryout. However, the panel recovered when the power was reduced to 400 watts.

Note that there is evidence of excess liquid in the corner 6, 24 in Figure 29. In order to check this, the opposite corner (7, 23) was lowered, as indicated in Figure 30. Thermocouple No. 6, which is on the upper surface, responded instantaneously and TC No. 24 on the bottom surface slowly recovered also. This test was not conclusive, however because this corner (6, 24) had been known to trap liquid at the lower fills also (see Figure 25). But in this case TC Nos. 17 and 29 slowly started to decrease in temperature with time as shown in Figure 31. When this corner (17, 29) was tilted upward there was a rapid recovery, indicating the presence of excess liquid in the panel.

It was concluded from these tests that a fill of 125 percent represents the optimum fill for this panel. This amounts to approximately  $1.43 \text{ lb}_m$  ( $0.65 \text{ kg}$ ) or  $0.07 \text{ lb}_m$  of methanol per square foot ( $355\text{g}/\text{m}^2$ ).

#### 5.3.4 Tilt Test

Next the heater was removed from the centerline of the panel and placed along one edge in order to perform the tilt test. The heater was bonded to the top surface just inboard of thermocouple Nos. 6, 10, 12 and 16 (see Figure 22). The purpose of this test was to demonstrate that the panel does operate properly even against a positive gravity loading. One side of the panel was always gravity aided, with the heater in the center, regardless of which direction the panel was tilted. Note, however, that a factor of four reduction in maximum heat transport is to be expected in this configuration. This is because all of the heat input must be transported over the full width of the panel. When the heater was in the center, only one-half of the heat load

TIME (3 DIVISIONS/HR)

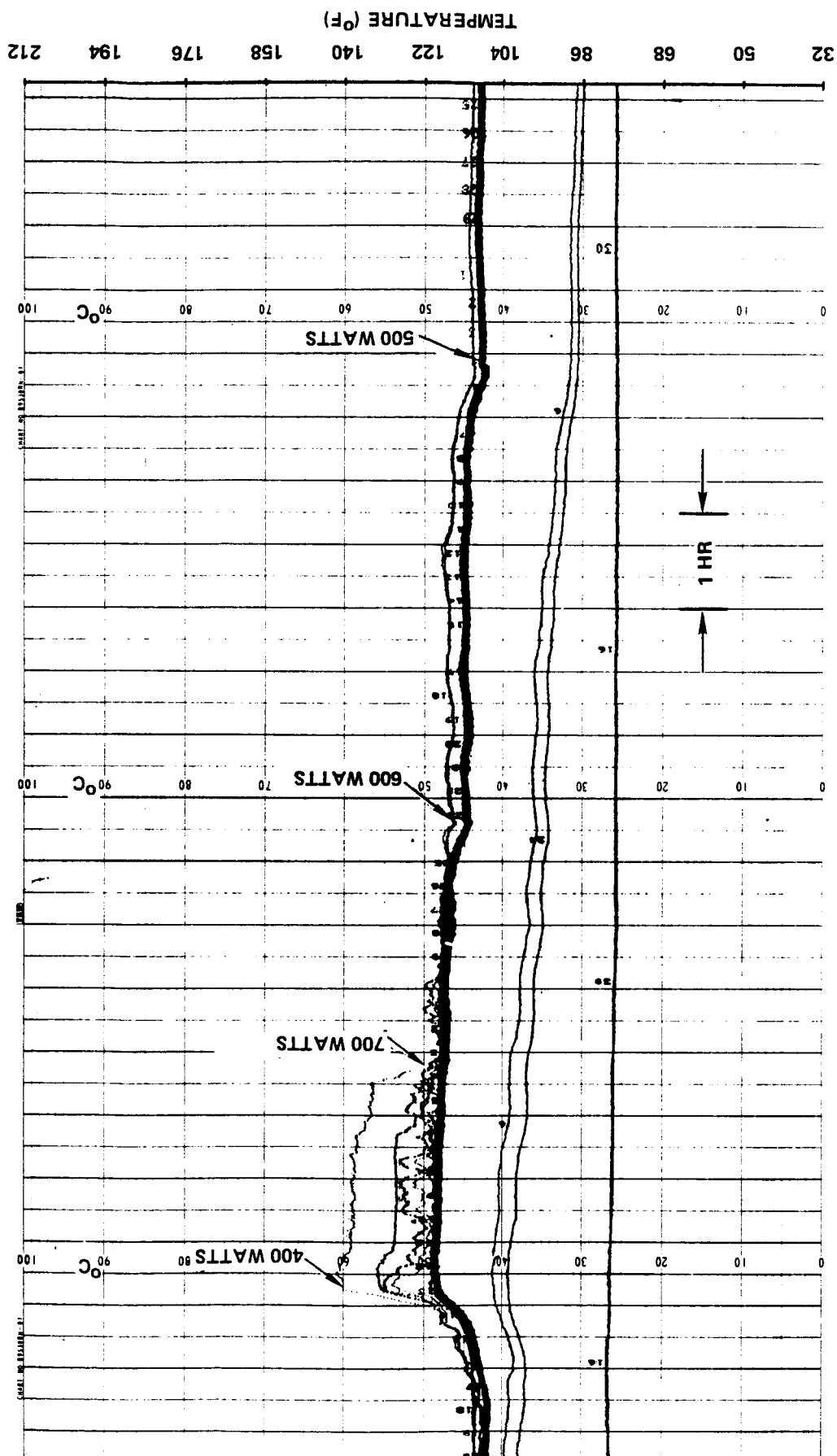


Figure 29 Maximum heat transport capacity test (130% fill).

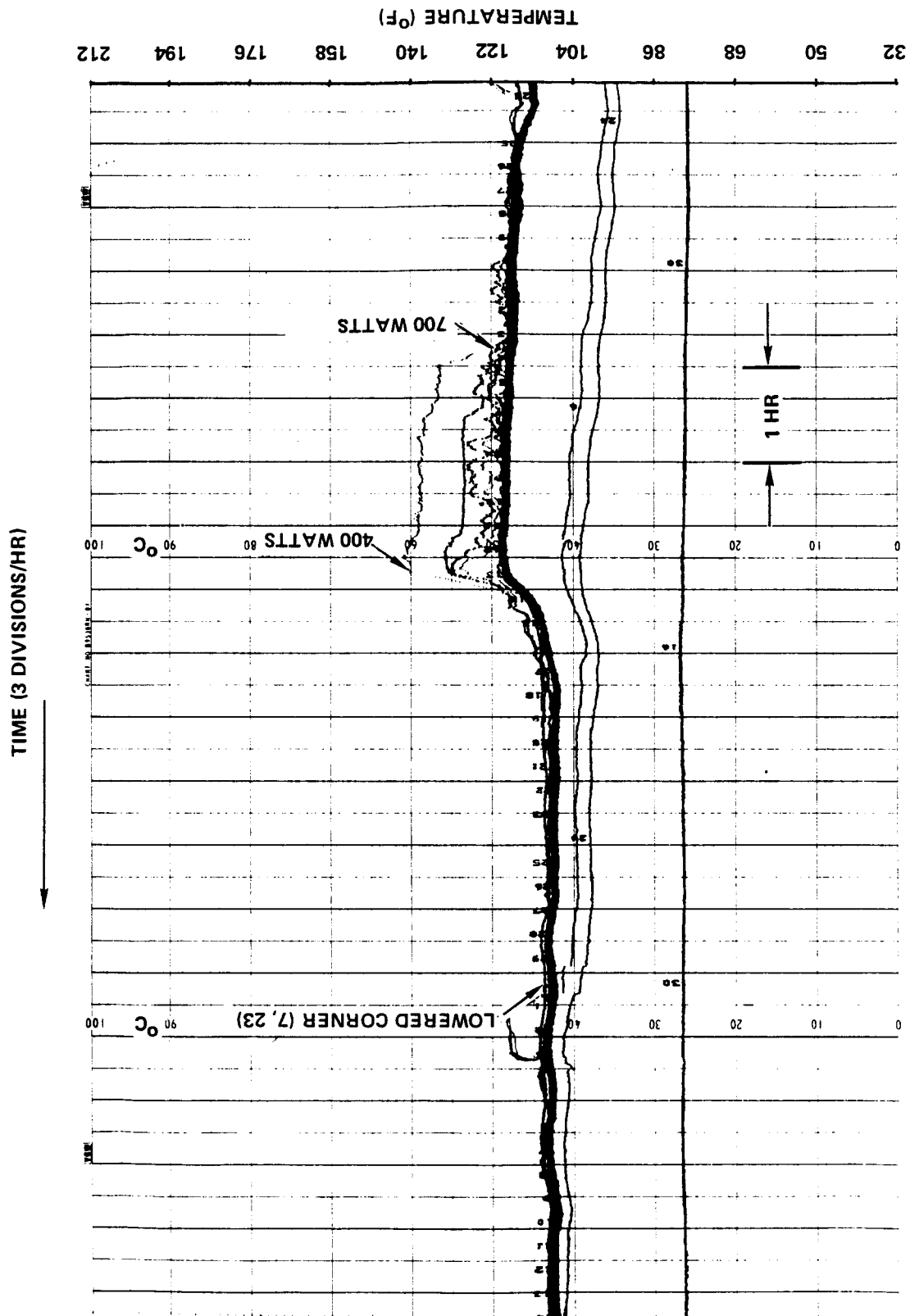


Figure 30 Verification of excess liquid in corner identified as 6, 24 (130% fill).

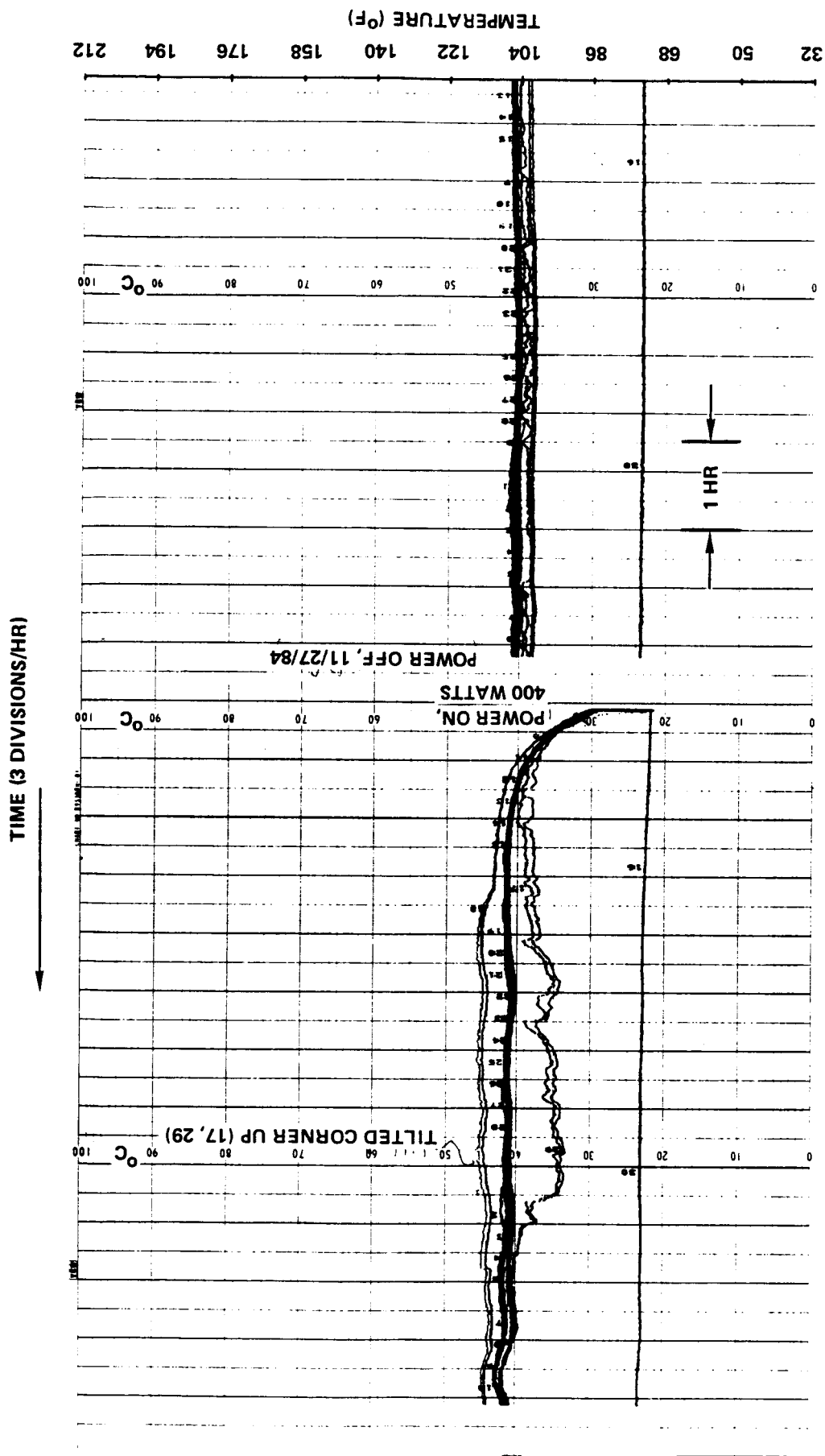


Figure 31 Verification of excess liquid in corner identified as 17, 29 (130% fill).

was required to be transported over one-half of the panel. Therefore, with no tilt and the heater located on the edge of the panel, maximum heat transport should be 150 watts.

This test was performed with the panel outside the test chamber using the room temperature ambient air as the heat sink. The tilt test results are plotted in Figure 32. In all cases, thermocouple Nos. 10 and 12 were the first to indicate dryout, followed by thermocouple Nos. 26 and 28. The lower data points represent steady state heat transport capability over a period of at least one hour, whereas the upper points indicate a temperature difference of greater than  $18.0^{\circ}\text{F}$  ( $10^{\circ}\text{C}$ ) between any two temperatures on the panel; i.e., dryout.

Although the maximum heat transport is lower than expected, these results verify the ability of the panel wicking system to successfully perform against an adverse gravity field. Because the curve "levels off" at low values of tilt, however, it is concluded that the reduced performance is due to a higher than expected vapor pressure drop. This will be discussed further under Data Correlation and Conclusions, in Section 6.0.

#### 5.3.5 Burst Pressure Test

The burst pressure test was performed on a subscale 5 1/2 inch by 5 1/2 inch (0.14 x 0.14 m) honeycomb panel. This sample was identical in materials and construction to the large thermal performance test panel. It was also constructed at the same time as the large panel. The test sample was helium leak checked before pressurizing.

Figure 33A shows the five locations where the sample thickness was measured. (Note that location No. 5 is not at the center, but at a point conveniently measured with technician's calipers.) First the thickness was measured in the free unpressurized state and recorded on the data sheet. The panel was then placed in a safety chamber and pressurized with ultra-pure nitrogen in 50 psig increments. After holding the pressure for ten minutes, the panel thickness was measured and recorded. The test data are summarized in Table 7. Between

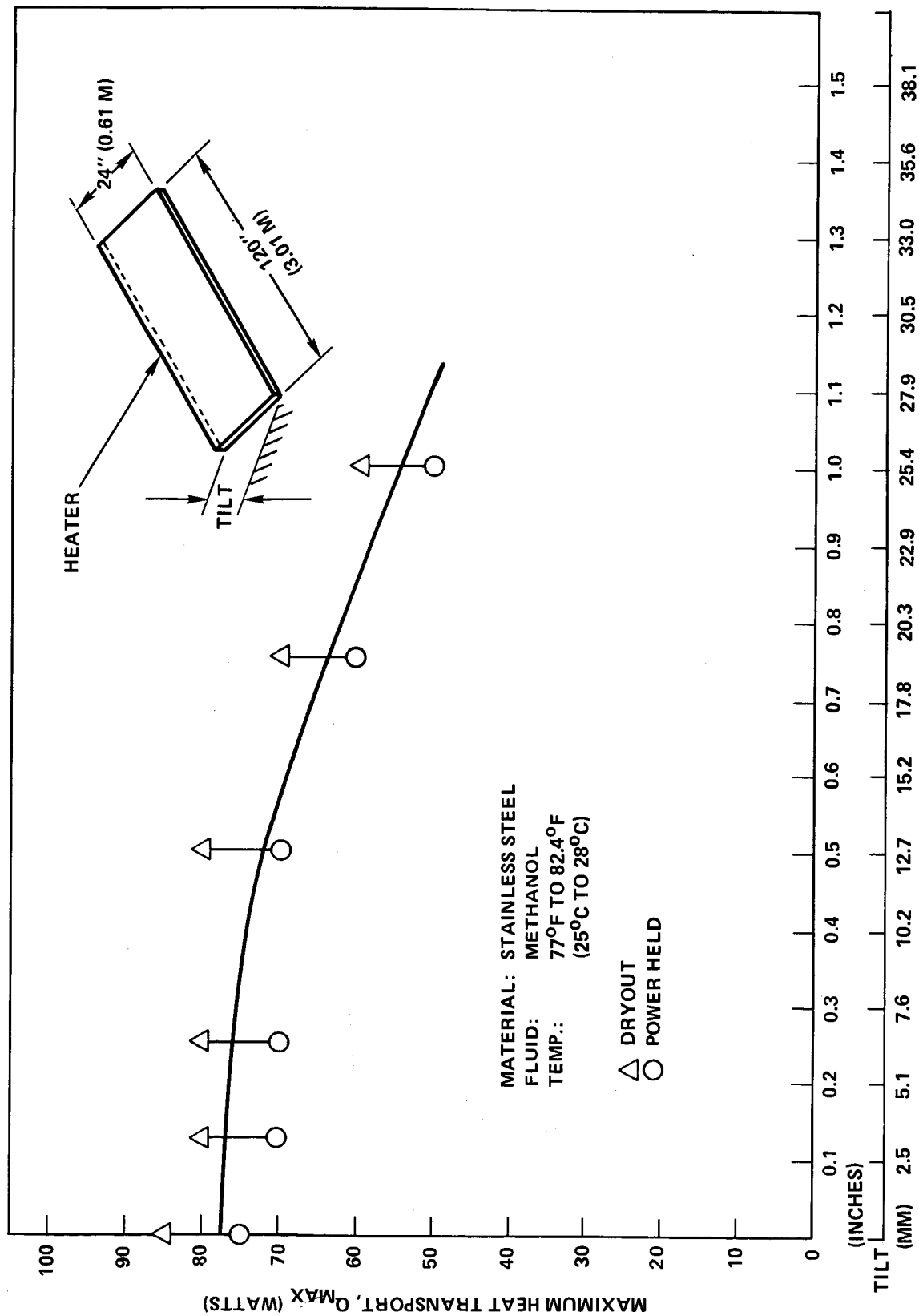
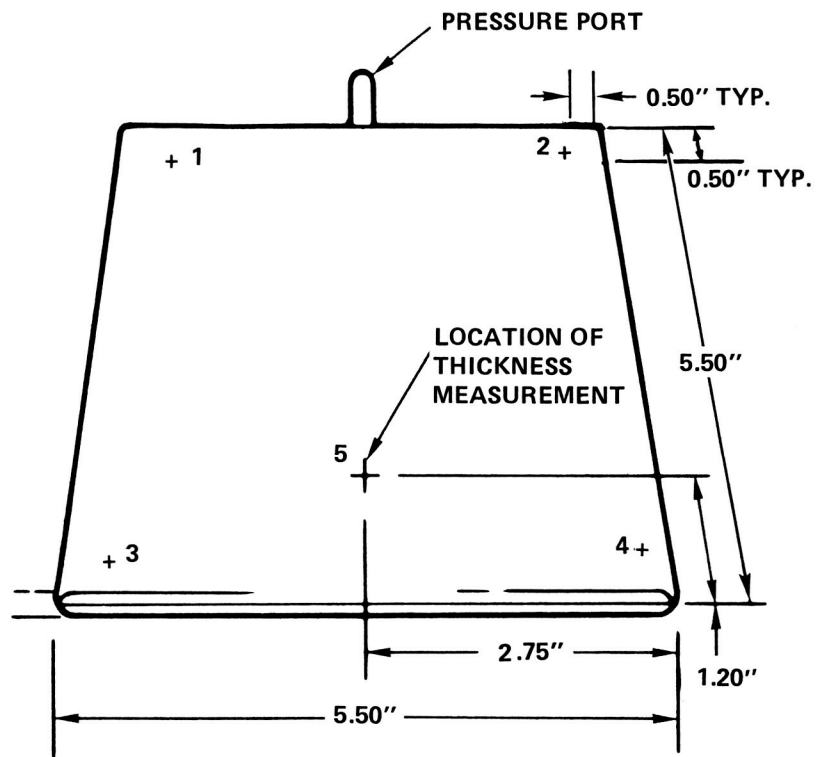
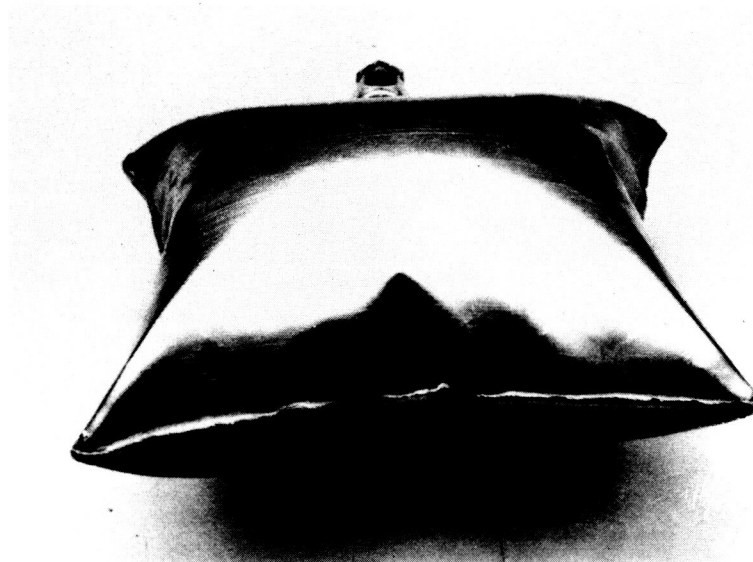


Figure 32 Honeycomb panel heat pipe tilt test performance.



A. BURST PRESSURE TEST SAMPLE DIAGRAM SHOWING MEASUREMENT LOCATIONS.

E4945



B. BURST PRESSURE TEST RESULT

Figure 33 Burst pressure test.



TABLE 7  
SUMMARY OF BURST PRESSURE DATA

Pressure (psig)	Thickness (in.)					Comments
	1	2	3	4	5	
0	0.311	0.310	0.311	0.311	0.314	
50	0.312	0.307	0.311	0.312	0.312	With pressure
100	0.311	0.309	0.312	0.312	0.314	With pressure
150	0.313	0.310	0.314	0.314	0.317	With pressure
200	0.316	0.315	0.318	0.321	0.322	With pressure
0	0.315	0.312	0.316	0.320	0.319	
250	--	--	--	--	--	Unit failed

each pressure point the sample was removed from the test chamber and helium leak checked to verify continued structural integrity.

At 200 psig a maximum deflection of .01 inch (0.25 mm) was observed. This deflection relaxed to only .009 inch (0.23 mm) when the pressure was vented to atmosphere, indicating permanent deformation. The sample was repressurized to 250 psig where, after approximately five minutes, the panel failed (Figure 33B). Subsequent examination of the panel, with a borescope inserted through the fill tube, revealed that the sintered wire core material had failed adjacent to the spot welds. Upon failure of the core material the unit expanded, like a "pillow". A leak check revealed two small leaks; one in the seam weld and one adjacent to the seam weld in a corner.

## 6.0 DATA CORRELATION AND CONCLUSIONS

### 6.1 Data Correlation

Subsequent to thermal performance testing, refinements were made in the honeycomb heat pipe thermal modeling, and software was created for the IBM PC-XT computer. The thermal transport model for the honeycomb fin was also upgraded to reflect as-built panel parameters described in Section 4.0. Basic analytic performance models for the honeycomb heat pipe were discussed in Section 3.0. Theoretical predictions aided the selection of design parameters to meet performance requirements. However, as previously mentioned, several important parameters differed between the as-designed and the as-built hardware. Table 8 compares preliminary design to actual parameters and summarizes their influence on predicted heat pipe transport capability. The thermal model was therefore upgraded, not only to incorporate actual parameters, but also to more accurately describe the complex physical geometry of the honeycomb panel and to expand its prediction capability.

#### Unit Cell Approach

A typical honeycomb panel consists of individual and repeatable cells. The liquid flow resistance of one such cell can be estimated by defining its physical constituents and using parallel and series flow path modeling. For the analysis, the approximately hexagonal cell shape is assumed to be square. The basic honeycomb cell has an "effective" flow resistance parameter described by:

$$\frac{L_1}{Aw_1 K_1}, \text{ defined as } C_1,$$

where:

$L_1$  = length (in liquid mass flow direction)

$K_1$  = permeability

$Aw_1 = W_1 H$ ;  $W_1$  = width,  $H$  = height

PRECEDING PAGE BLANK NOT FILMED

TABLE 8  
SUMMARY OF ANALYSIS UPGRADING

Parameter	Value		Effect
	Pre-Fab.	Actual	
Vapor flow area	0.012 in <sup>2</sup> (7.92 mm <sup>2</sup> )	0.0031 in <sup>2</sup> (1.98 mm <sup>2</sup> )	Decrease $Q_{\text{Sonic}}$ Decrease $Q_{\text{Entrainment}}$ Increase $\Delta P_v$ ; Decrease $Q_{\text{Wicking}}$
Vapor path length (along one "channel")	12 in (0.30 m)	16.9 in (0.43 m)	Increase $\Delta P_v$ ; Decrease $Q_{\text{Wicking}}$
Spotweld spacing:	Percent Open:		
Mini flange to facesheet	25	~10	Increase $\Delta P_\ell$ ; Decrease $Q_{\text{Wicking}}$
Cell interfaces	25	100	Decrease $\Delta P_\ell$ ; Increase $Q_{\text{Wicking}}$
Resulting in:			
Unit cell flow resistance parameter (Cl)	$3.58 \times 10^{13} \text{ m}^{-3}$	$4.95 \times 10^{13} \text{ m}^{-3}$	
Fluid tortuosity factors	$TF_v = 1.0$ $TF_\ell = 1.0$	$1.0 \geq TF_v > 0$ $1.0 \geq TF_\ell > 0$	Increase $\Delta P_v$ ; Increase $\Delta P_\ell$ ; Both decrease $Q_{\text{Wicking}}$
Effective capillary pore radius	$r_c = 23 \times 10^{-6} \text{ m}$ (165 x 1400 core wick)	$23 \times 10^{-6} \text{ m} \leq r_c$ $\leq 84.9 \times 10^{-6} \text{ m}$ (120 x 120 facesheet wick)	Reduce $\Delta P_c$ ; Decrease $Q_{\text{Wicking}}$

Using this "unit cell" parameter in a building block fashion (see Figure 34), the total flow resistance of a complete honeycomb panel can be calculated.

Parallel to flow direction:

$n$  additional cells will multiply;

$C_1 n$  (added flow length)

Perpendicular to flow direction:

$n$  additional cells will divide;

$C_{1/n}$  (flow splitting)

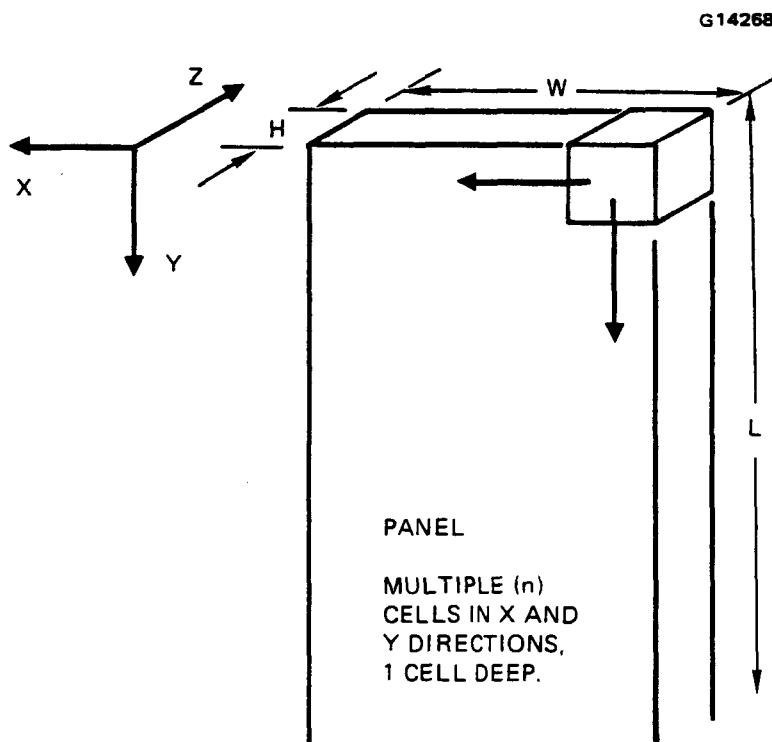


Figure 34 Honeycomb panel shown as comprised of "unit cells".

$$\left[ \frac{L}{AwK} \right]_{\text{panel}} = \left( \frac{L_1}{Aw_1 K_1} \right)_{\text{unit cell}} \left( \frac{L}{L_1} \right) \left( \frac{1}{Aw/Aw_1} \right)$$

$$= C_1 \left( \frac{L}{L_1} \right) \left( \frac{Aw_1}{Aw} \right)$$

The unit cell approach was introduced into the wicking transport equations of the computer model. It permits easy interchange of variable panel sizes, evaporator and condenser locations, and direction of heat flow.

### Tortuosity Factors

The effect of fluid flow "tortuosity" in its complex travel path through each honeycomb cell has not been fully included in the analytic model. In reality, sudden fluid flow bending, enlargement, contraction, etc., will add to the total pressure drop and thus act to reduce the wicking transport capability. The computer model permits independent selection of liquid ( $TF_\ell$ ) or vapor ( $TF_v$ ) tortuosity factors. Values ranging from unity (no flow obstruction) to zero (complete flow obstruction) can be used to correlate localized pressure drop magnification ( $MF \Delta P$ ):

$$TF = 1/MF \Delta P$$

### Composite Wick Considerations

The honeycomb core consists of a composite wick structure, i.e., the facesheet and core ribbon wicks have different pumping pore radii ( $r_c$ ) and permeability ( $K$ ) characteristics. Specific  $r_c$  and  $K$  values have been experimentally determined for a previous honeycomb panel (Ref. 10) having identical composite wicks as used in this panel. Although the analytic model accounts for the varied permeability between alternate liquid flow paths, it is not certain

which pore radius governs the capillary pumping. Since the heat input is into the facesheet, it seems that this is the pore most likely to govern pumping.

An upgraded performance prediction for the  $-4$  to  $149^{\circ}\text{F}$  ( $-20$  to  $65^{\circ}\text{C}$ ) temperature range is shown in Figure 35. Approximately a four to one variance in the capillary limit is possible as a result of selecting the high or low pore radius. Performance curves are also shown which assume independent existence of facesheet wick only or of core ribbon wick only; these are useful in establishing absolute minimum thermal transport capacities.

Table 9 shows pressure drops predicted by analytic performance model for three temperature levels. The relative significance of vapor pressure drop varies significantly over the radiator operating temperature range; from being the largest contributor at low temperatures to relatively insignificant at higher temperatures. Maximum thermal transport results from the various tests are shown as a function of fluid temperature in Figure 36. The performance uses the conservative pumping pore radii-case 2 (Ref. Figure 35) and this is plotted as baseline. The independent influences of liquid and vapor tortuosity factors are also plotted. At the 75 percent level (implying a localized pressure drop increase of 33 percent), the vapor tortuosity factor correlates to test data at low temperatures, while the liquid tortuosity conservatively correlates at higher temperatures.

Tilt test results are shown as a function of fluid temperature in Figure 37. Test results correlate to a combined (vapor plus liquid) tortuosity factor of about 0.8 for the larger tilt heights. However, the actual performance levels off at low values of tilt. This may be explained by vapor flow effect, not included in the model.

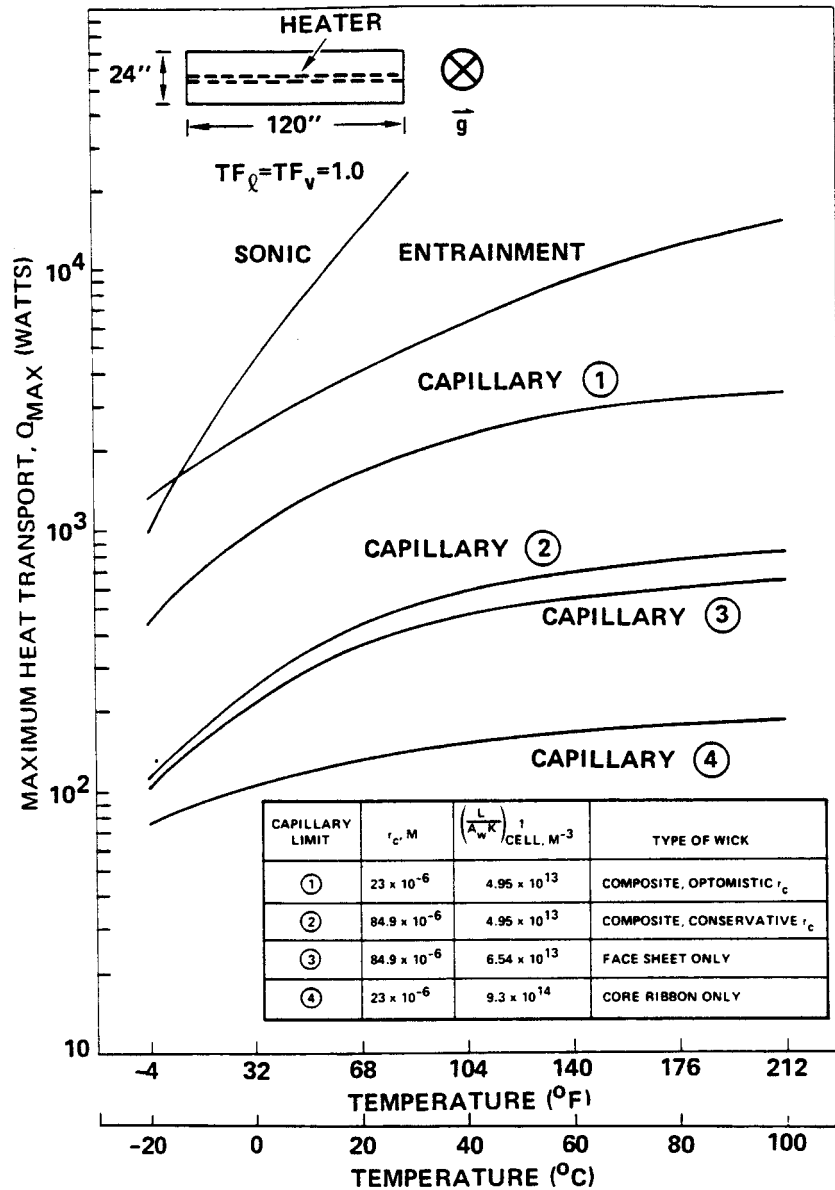


Figure 35 Predicted performance limits upgrade for stainless steel/methanol honeycomb heat pipe.

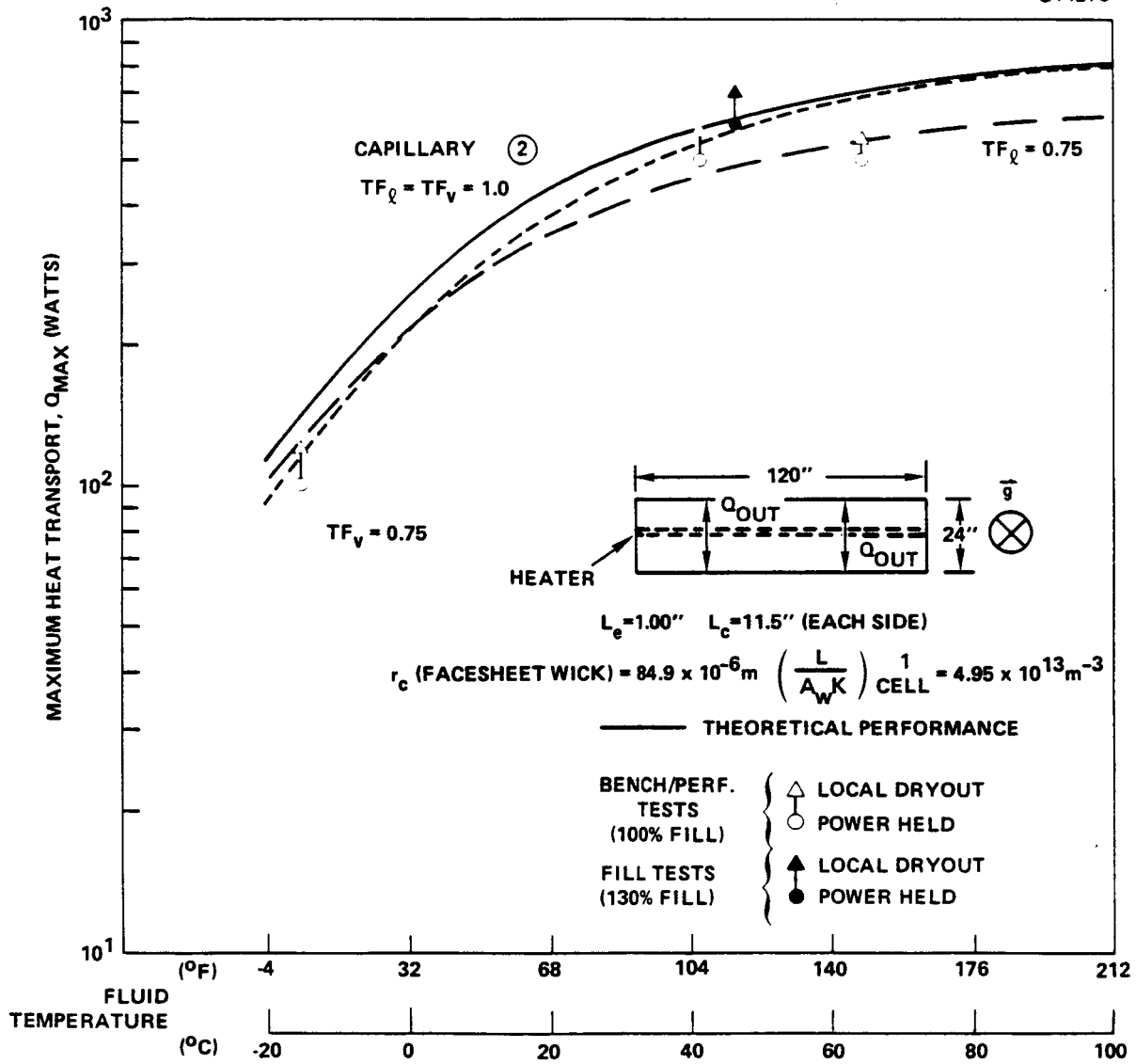


Figure 36 Data correlation: thermal transport limitation.



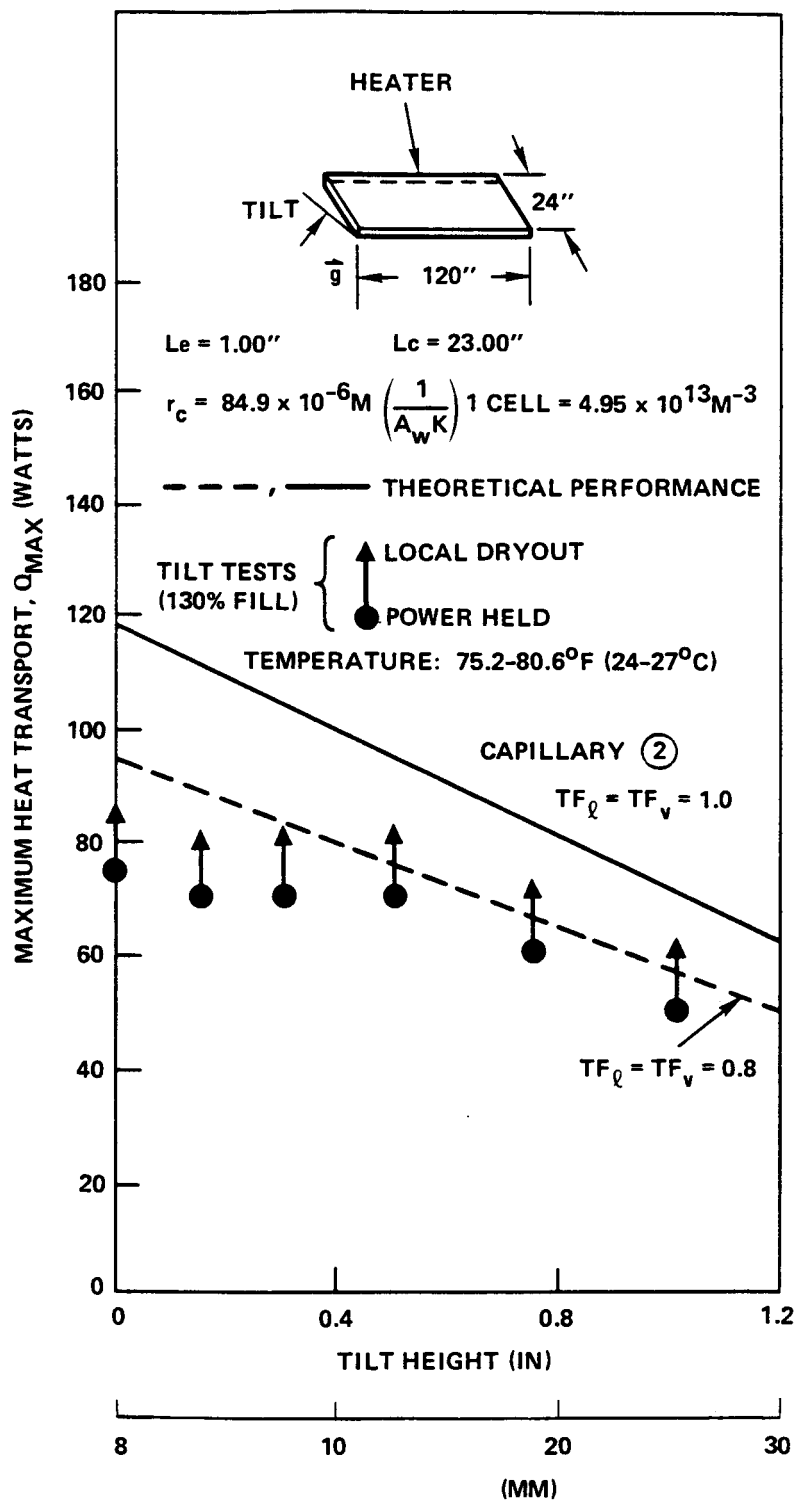


Figure 37 Data correlation: tilt test performance.

TABLE 9  
SUMMARY OF PREDICTED PRESSURE LOSSES

G14272

LOSS TERM	T=30.2°F	Q=246W	T=100.4°F	Q=557W	T=170.6°F	Q=780W
	$\Delta P, N/m^2$	% TOTAL	$\Delta P, N/m^2$	% TOTAL	$\Delta P, N/m^2$	% TOTAL
GRAVITY	50.6	8.6	48.3	9.5	45.9	10.7
HONEYCOMB CORE LIQUID	253.0	42.8	357.0	70.5	346.0	81.1
HONEYCOMB CORE VAPOR	287.0	48.6	101.0	20.0	34.8	8.2
TOTAL	590.6	100.0	506.3	100.0	426.7	100.0

## 6.2 Conclusions

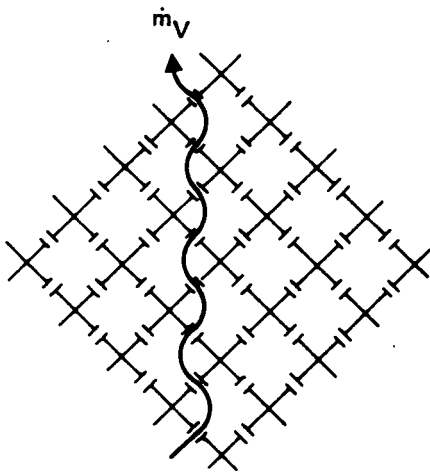
The major objective of this honeycomb heat pipe development program was to demonstrate performance for the space radiator fin application. The feasibility of fabricating and processing a stainless steel heat pipe in a honeycomb configuration for the fin application has been successfully established. A heat transport capacity of 600 watts at 122°F (50°C) or 60 watts per foot (200 watts per meter) of fin length was demonstrated. This falls short of the design goal of 1,000 watts, primarily because the vapor holes were punched by the vendor only in every other crimp of the core wick material, rather than every crimp as originally specified (see Figures 15 and 18).

A close look at the test panel interior reveals constraints placed on its performance and helps explain test results. This is illustrated in Figure 38 which shows the several possible vapor flows resulting from alternate placement of holes in the core ribbon. With holes in every honeycomb cell face, as originally designed, the vapor can communicate between all cells and can work

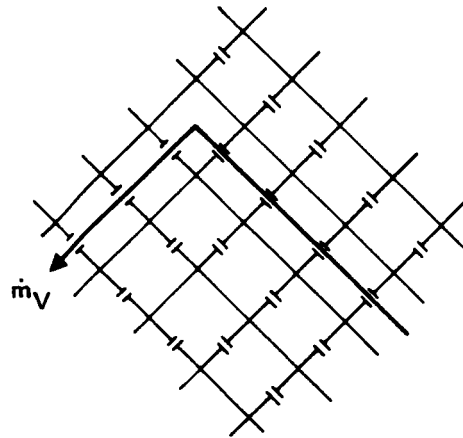
its way from any evaporator location to a point directly opposite it on a condenser edge (see Figure 38a). As mentioned previously, the vapor flow area and length were adversely affected due to the inclusion of vapor holes in every other crimp only, rather than in every crimp (Ref. Figure 18). If the holes of adjacent core ribbon strips are in phase as in Figure 38b, the vapor will flow diagonally across the entire panel. If however, the adjacent strip of core material is shifted one cell as shown in Figure 38c, vapor will be forced to take a  $90^\circ$  turn in a following cell, depending on how adjacent strips are lined up.

Holes punched into the core ribbon constrain the vapor to flow along paths which can be viewed as "channels." The test panel actually consists of three sections which differ in arrangement of those vapor channels. The left and right sections contain single direction channels, but are oriented  $90^\circ$  out of phase with each other. The middle section is comprised of a mix of channel sections creating very complicated vapor flow. Although the core ribbon wick material is permeable to vapor - if given sufficient time to pass through - it does severely diminish its ability to freely and rapidly communicate with all areas of the panel. As a result, the full radiator area is not utilized effectively, as shown in the detail schematic of the middle core section (Figure 39). The areas above the top shaded channel (for center heater) and the area above the bottom shaded channel (for edge heater) are cut off from "free" vapor flow and therefore become non utilized or poorly utilized sections of the heat pipe condenser. Similarly, the panel corners at TCs 16, 30 and 6, 24 are isolated from vapor by continuous channel walls - if the heater is centrally located as during baseline, performance, and fill tests. Since these corners are thermally isolated, they become subcooled relative to the rest of the panel; differences in vapor pressure will thus cause liquid to fill them. Under conditions that create cold corners, excess working fluid will be required to prevent premature panel dry-out. When the heater was relocated to the panel edge during tilt testing, these cold corners did not reappear.

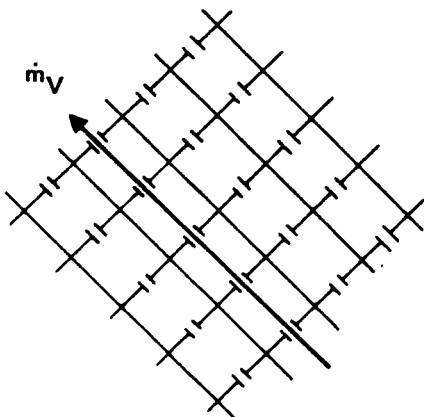
Severe localized effects are possible within fluid channels of the middle panel section. These are: the same channel can cross under the heater several times and thus receive multiple heat loads; vapor pressure drops will increase



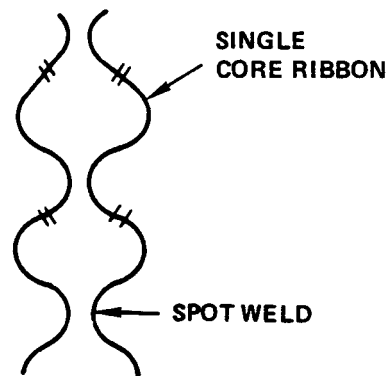
A. ORIGINALLY DESIGNED



C. AS BUILT; OUT-OF-PHASE SECTION



B. AS BUILT; IN-PHASE SECTION



ACTUAL CELL SHAPE  
(OUT-OF-PHASE CORE  
RIBBON JOINING SHOWN)

NOTE: TOP PANEL VIEW SHOWN

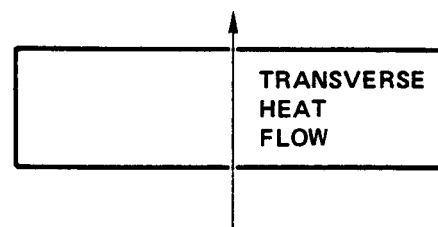


Figure 38 Summary of cell hole pattern effect on vapor flow direction.

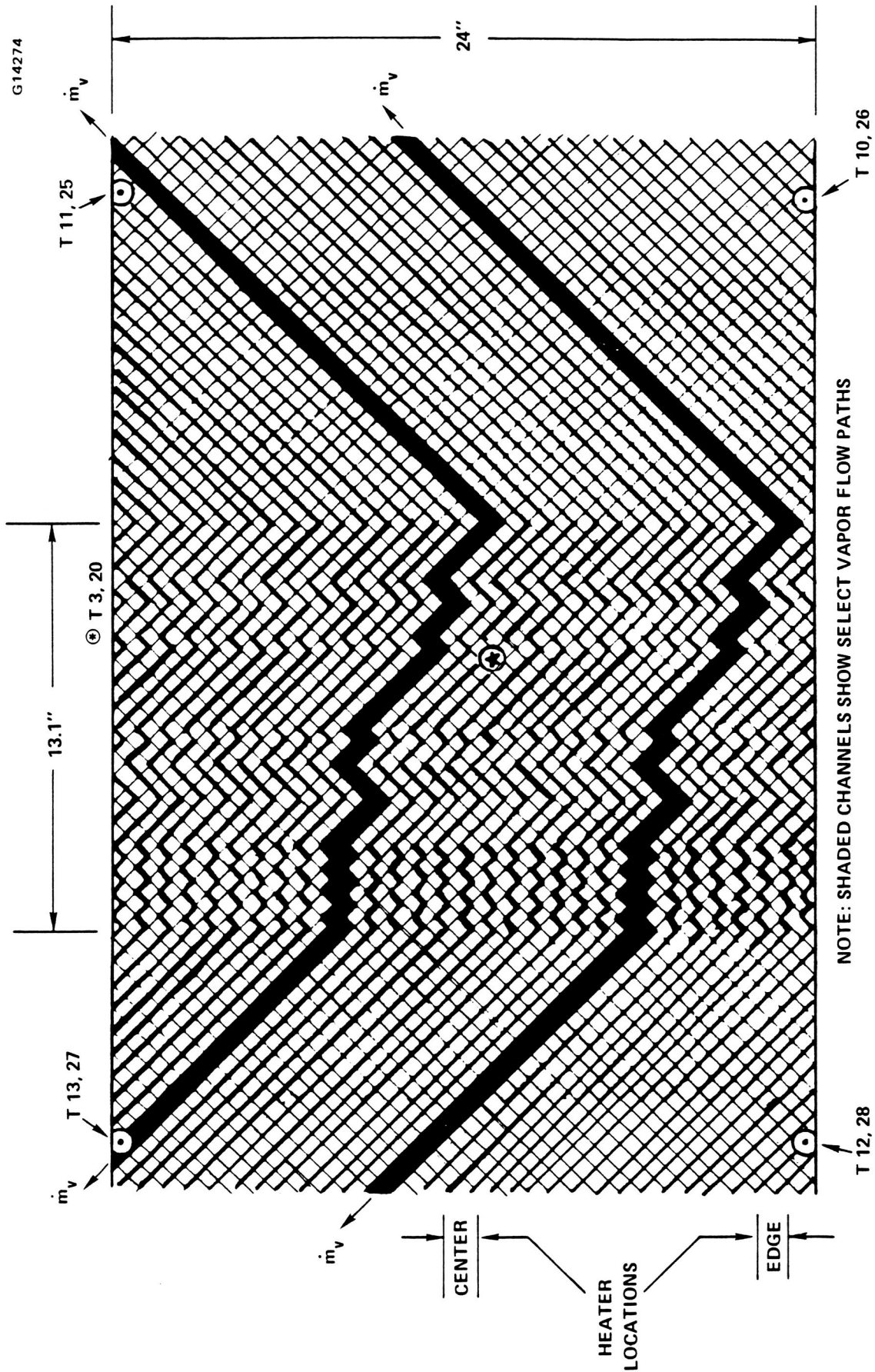


Figure 39 Detail view of panel section having mixed directions channels.

due to numerous changes in flow direction and from longer flow paths; and entrainment and sonic limits will be depressed by effective reductions in vapor flow area. In most cases, initial dry-out was observed at evaporator thermocouples located nearest the troublesome middle panel section (TC for central heater and TC's 10,12 for edge heater); the region where multiple heat loading exists.

The current analytic model incorporates single-directional channel characteristics shown in Figure 38b only, in other words, the complications of the middle channel section are not included. Although greater prediction accuracy can be developed, it would be a time-consuming task. The preferred approach is to ascertain that future honeycomb panels have adequate vapor communications and thus utilize the existing correlated model to predict performance. This is done for the two additional cases, as shown in Figure 40. The upper curve shows the increase in as-designed panel performance, which incorporates a four-fold increase in vapor flow area and 50 percent open liquid flow area at facesheet spotwelds. Leveling of the curve is a result of the relative significance of vapor as compared to liquid pressure drops at lower temperatures. However, to meet the design goal of 1000 watts over the entire operating temperature range shown in the upper curve, it is necessary to incorporate the lower flow resistance of honeycomb channels. Both cases use combined tortuosity factors of 0.8, which is very conservative for the channel design.

The conclusions based on results of this development program are summarized below:

- Acceptable fabrication and processing techniques of stainless steel/methanol heat pipes in a honeycomb configuration for the space radiator fin application have been developed.
- A heat transport capacity of 600 watts or 60 watts per foot (197 watts/meter) of fin length was demonstrated. This falls short of the 1000 watt design goal, primarily because vapor holes were punched in every other crimp of the core ribbon only, rather than every crimp as originally designed.

due to numerous changes in flow direction and from longer flow paths; and entrainment and sonic limits will be depressed by effective reductions in vapor flow area. In most cases, initial dry-out was observed at evaporator thermocouples located nearest the troublesome middle panel section (TC for central heater and TC's 10,12 for edge heater); the region where multiple heat loading exists.

The current analytic model incorporates single-directional channel characteristics shown in Figure 38b only, in other words, the complications of the middle channel section are not included. Although greater prediction accuracy can be developed, it would be a time-consuming task. The preferred approach is to ascertain that future honeycomb panels have adequate vapor communications and thus utilize the existing correlated model to predict performance. This is done for the two additional cases, as shown in Figure 40. The upper curve shows the increase in as-designed panel performance, which incorporates a four-fold increase in vapor flow area and 50 percent open liquid flow area at facesheet spotwelds. Leveling of the curve is a result of the relative significance of vapor as compared to liquid pressure drops at lower temperatures. However, to meet the design goal of 1000 watts over the entire operating temperature range shown in the upper curve, it is necessary to incorporate the lower flow resistance of honeycomb channels. Both cases use combined tortuosity factors of 0.8, which is very conservative for the channel design.

The conclusions based on results of this development program are summarized below:

- Acceptable fabrication and processing techniques of stainless steel/methanol heat pipes in a honeycomb configuration for the space radiator fin application have been developed.
- A heat transport capacity of 600 watts or 60 watts per foot (197 watts/meter) of fin length was demonstrated. This falls short of the 1000 watt design goal, primarily because vapor holes were punched in every other crimp of the core ribbon only, rather than every crimp as originally designed.

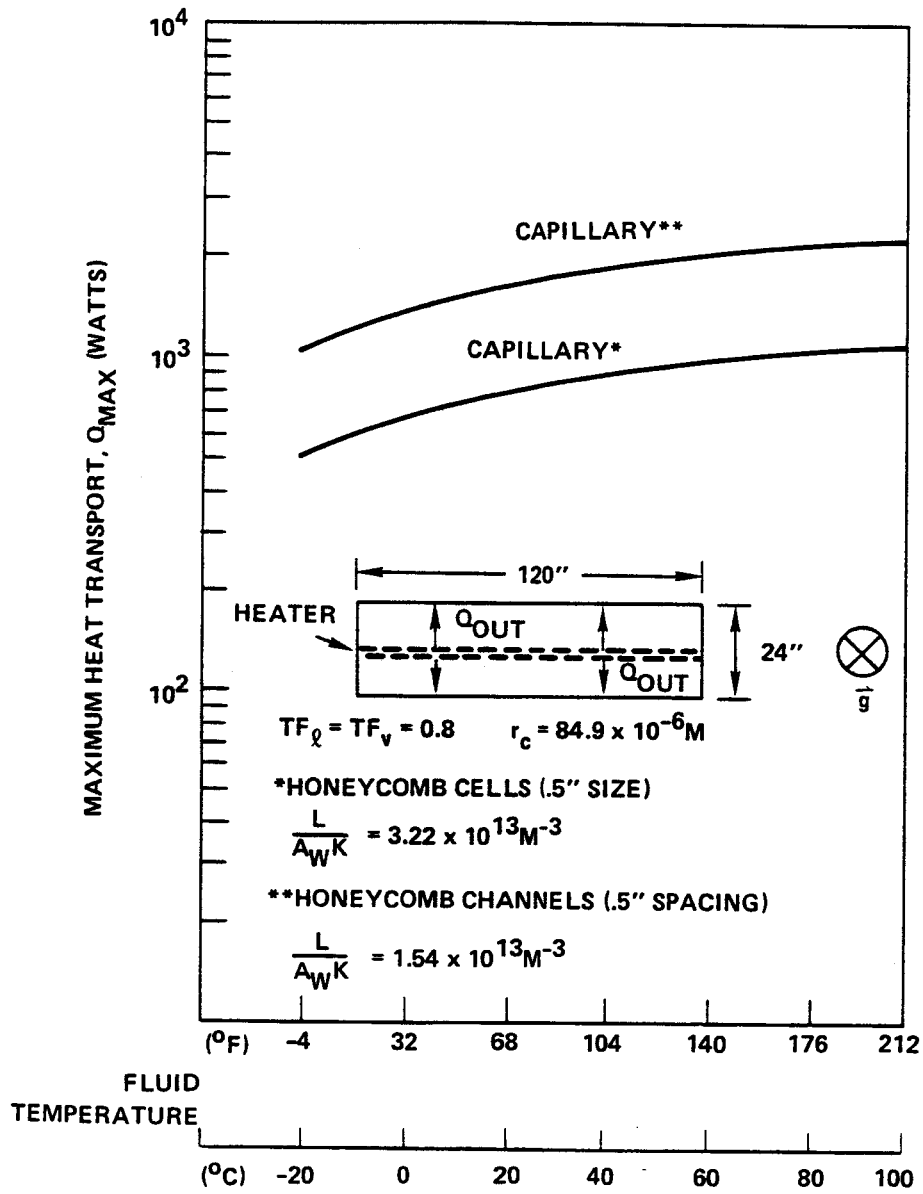


Figure 40 Predictions for as-designed and increased capacity designed using correlated model.



- A temperature differential of  $\pm 2.7^{\circ}\text{F}$  ( $1.5^{\circ}\text{C}$ ) (at 600 watts) over the entire active surface of the honeycomb panel was demonstrated. The existence of two small cold corners is due to vapor isolation created by core ribbons without vapor holes.
- The inclusion of vapor holes in every core ribbon crimp will ensure the necessary vapor communication throughout all areas of the honeycomb panel and will result in the panel exceeding all performance requirements.
- The correlated analytic model can be used with subscale panel segment tests to predict performance of future panel hardware. As-designed panel performance is predicted to be from 500 to 1000 watts over the operating temperature ranges; an open channel design is predicted to achieve greater than 1000 watts over the entire temperature range.
- The panel can operate over a wide temperature range without liquid blockage effects due to liquid expansion. The honeycomb core material inherently provides excess liquid reservoir capacity distributed throughout the panel.

The technology and commercial equipment are currently available to construct all-welded, machine-assembled heat pipe panels using stainless steel and other ferrous materials, nickel alloys, titanium, and titanium alloys. Aluminum panels will require further development of these techniques and/or alternative methods of fabrication.

An improved lightweight heat pipe radiator fin will evolve from additional efforts to reduce weight and maintain the panel within structural allowables. Fabrication processes for lightweight aluminum, low density wickable core honeycomb panels require further evaluation. Channel and strut designs could provide improved performance. Modular design trade-offs must be evaluated to essentially isolate panel compartments, and provide high reliability to micro-meteoroid and space debris damage.

## REFERENCES

1. Ellis, W.E., and Rankin, J.G., "Heat Rejection Development Requirements for Orbital Power Systems", Paper No. 799295, 14th Intersociety Energy Conversion Engineering Conference, August 1979.
2. Oren, J.A., "Study of Thermal Management for Space Platform Applications," NASA CR-165238, December 1980.
3. Oren, J.A., "Study of Thermal Management for Space Platform Applications: Unmanned Module Thermal Management and Radiator Technologies," NASA CR-165307, May 1981.
4. Rankin, J.G., and Marshall, P.F., "Thermal Management System Technology Development for Space Station Applications," Paper No. 831097, 13th Intersociety Conference on Environmental Systems, July 1983.
5. Basiulis, A., and Camarda, C.J., "Design, Fabrication and Test of Liquid Metal Heat-Pipe Sandwich Panels," AIAA Paper No. 82-0903, AIAA/ASME 3rd Joint Thermophysics, Fluids, Plasma & Heat Transfer Conference, June 1982.
6. Tanzer, H.J., "High Capacity Honeycomb Panel Heat Pipes for Space Radiators," AIAA Paper No. 83-1430, June 1983.
7. Alario, J., Haslett, R., and Kosson, R., "The Monogroove High Performance Heat Pipe", AIAA Publication 81-1156, June 1981.
8. Tanzer, H.J., "Fabrication and Development of Several Heat Pipe Honeycomb Sandwich Panel Concepts", NASA CR 165962, June 1982.
9. Fleischman, G.L., Scollon, T.R., and Loose, J.D., "Vapor Chambers for an Atmospheric Cloud Physics Laboratory," AIAA Paper No. 82-0903, July 1980.
10. Camarda, C.J., and Basiulis, A., "Radiant Heating Tests of Several Liquid Metal Heat-Pipe Sandwich Panels," AIAA Paper No. 83-0319, January 1983.
11. Experimental Data for Flat-Plate Heat Pipes, Unpublished, Hughes Aircraft Company, Electron Dynamics Division, CA.